Theoretical study of CO oxidation on Au nanoparticles supported by MgO(100)

L. M. Molina and B. Hammer
iNANO and Department of Physics and Astronomy, University of Aarhus, DK-8000 Aarhus C, Denmark
(Received 7 August 2003; revised manuscript received 20 January 2004; published 22 April 2004)

We present a density-functional-theory (DFT) study of the reactivity towards CO oxidation of Au nanoparticles supported by MgO(100). We model two geometrical aspects of the Au particles, the low index facets of the Au particles, and the Au-MgO interface boundary. The precise structure of the interface boundary depends on the size of the Au particles, and different models with either small or large Au-MgO contact angles are introduced. For all Au systems, we find that the CO oxidation reaction proceeds via CO adsorption, trapping of O_2, leading to the formation of a metastable $CO \cdot O_2$ reaction intermediate, which dissociates into CO_2 and adsorbed atomic oxygen. The atomic oxygen reacts directly with gas phase CO. No separate O_2 molecular or dissociative adsorption is found to be favorable. Important differences were found in the reactivity of the various Au-MgO interface boundaries. This is explained in terms of two properties: the Au-Au coordination determining the local reactivity of the Au atoms and the presence of the MgO support that, besides providing excess electrons to the Au clusters, forms ionic bonds to the peroxo part of the $CO \cdot O_2$ reaction intermediate. We find that the type of interface boundary likely to be predominant for medium-sized nanoparticles provides the optimal degree of low-coordinated Au atoms in the neighborhood of the MgO support. Our DFT study therefore provides a rational for why the reactivity per site may reach a maximum at a critical particle size as has been observed experimentally for similar systems.

DOI: 10.1103/PhysRevB.69.155424 PACS number(s): 68.47.Jn, 82.65.+r, 68.43.Fg, 68.35.Np

I. INTRODUCTION

The possibility of using supported Au nanoparticles as efficient catalysts at low temperatures has attracted an enormous interest, since the discovery in 1987 by Haruta[1,2] of high reactivity towards CO oxidation in gold deposited on various metal oxides at and below room temperature. Also, oxide-supported Au catalysts were recently found to be active for a number of interesting reactions, such as propene epoxidation,[3] reduction of nitrogen oxides,[4] and dissociation of SO_2.[5] A vast amount of experimental works have studied the origin of this reactivity as well as the influence of several factors (particle size, substrate, method of preparation, etc.) on the catalysts performance.[6] A key factor to influence reactivity is the particle size. On a variety on supports, Au particles have been extensively reported to only become reactive at sizes below ≈ 5 nm.[7,8] More interestingly, Goodman and co-workers[9] have even observed an optimum particle size of ≈ 3 nm diameter for the low-temperature combustion of CO on Au model catalysts supported on a TiO_2 surface. They also noted that these clusters appear to be only 2–3 Au layers thick. In addition, Bondzie *et al.* found that the adsorption of atomic oxygen on small Au particles becomes stronger as the size of the particles decreases.[10] The high activity of such very small particles has been interpreted by Mavrikakis *et al.*[11] in terms of the enhanced proportion of low-coordinated sites (edges, corners) at the cluster surface; their simulations show a clear correlation between decreasing Au coordination and enhanced adsorbate binding strength. Recent calculations for a free Au_{10} cluster by Lopez and Nørskov have further confirmed this point.[12]

Together with the particle size, the nature of the arrangement of the particles seems to be crucial. Haruta has pointed out indications of a superior performance of hemispherical particles strongly attached to the substrate, in contrast to other more spherical shapes with lower reactivities for comparable average sizes.[13] Recently, Pietron *et al.*[14] have shown that relatively large (~ 6 nm) Au particles can be very active on Au-TiO_2 aerogels due to the enhancement of the Au/TiO_2 contact area. These facts give strong support to the hypothesis of the Au/substrate interface boundary as the active region for CO oxidation.[15] Further support to this idea comes from the fact that sizable differences in reactivity are observed between particles of similar size supported on different substrates.[7]

Despite all these advances, many aspects related to the mechanisms of the reaction and the detailed nature of the active sites are still under debate. Consequently, we have decided to perform a theoretical study based on density-functional theory (DFT) of the reactivity towards CO oxidation on supported gold clusters, with particular emphasis on the behavior of the particle-substrate interfacial region. The DFT method has previously been used successfully for the description of CO oxidation over transition- and noble-metal surfaces.[16–23] We have chosen MgO as support for a number of reasons. First, its structural simplicity makes it very suitable for computational purposes since it provides great flexibility when choosing the computational cell and allows for the use of rather thin supporting slabs. Second, nanometer-(nm) sized Au clusters on MgO show sizable activities,[24] again at small sizes (2–3 nm). Finally, very small (of the order of tens of atoms) Au clusters on MgO have also been shown to be active by Sanchez *et al.*[25] In this latter case, the role of the oxide as something more than a mere structural promoter has been identified and discussed in terms of charge transfer from the support to the metallic clusters. Charging of these tiny clusters in the gas phase has been found important for their ability to bind and activate O_2, both theoretically[26,27] and experimentally.[28]

The paper is outlined as follows. First, we will describe

the construction of the models employed for Au clusters in the study of their reactivity. The arrangement of the clusters on the substrate is not a trivial matter, and we therefore present the results for a range of Au systems (atoms, dimers, thin films, and rods) in various positions and configurations over the MgO(100) surface. Second, the reactivity of a number of different sites around supported 2D (two-dimensional) and 3D particles will be studied, including Au(100) and Au(111) facets, a 2 ML (monolayer) thin film, and edges both in close contact with the substrate and far away from it. This covers most of the surface of the possible particles, with the only exception of cluster corners. The reactivity of such sites is expected, however, to be comparable to that of the cluster edges included in our study. The 2D thin-film structure is included, despite the experimental evidence that 3D structures are more likely to form, since we find it interesting from a fundamental point of view to evaluate the effects of the reduced dimensionality of Au. 2D growth may be important for other substrates, judging, e.g., from Goodman and co-workers[9] who conclude the most reactive Au clusters found on a TiO_2 surface to be only 2–3 Au layers thick. Finally, we will perform an extensive analysis of the results obtained, and of the several effects found due to the presence of the substrate. A brief account of parts of the present work was recently given elsewhere.[29]

II. MODEL

The *first-principles* DFT calculations are performed using a plane-wave basis set,[30] ultrasoft pseudopotentials,[31] and a spin-polarized, nonlocal density gradient approximation for the treatment of exchange-correlation (XC) effects. An energy cutoff of 25 Ry is employed for the plane-wave expansion of the wave functions. We will mainly discuss the results in terms of the revised Perdew-Burke-Ernzerhof (RPBE) XC functional,[32] since this functional seems to be more reliable for the description of molecular binding energies and bonding of adsorbates to surfaces.[32,33] For consistency with the literature however, and in order to show that most of the results and conclusions are independent of the choice of functional, we provide the energetics calculated using the Perdew-Wang-91 (PW91) XC functional[34] as well. For the calculations of 2D thin layers, truly self-consistent PW91 energies and non-self-consistent RPBE values are reported, whereas in the case of 3D clusters, truly self-consistent RPBE energies are given. We have checked that the results are independent of which functional is chosen for self-consistency (that is, non-self-consistent RPBE energies are calculated typically to be within 0.03 eV of the truly self-consistent values). Test calculations for simple molecules show a great improvement in the comparison with experimental binding energies when using the RPBE rather than the PW91.[33] In Table I we report the calculated binding energies of CO, O_2, and CO_2, and the resulting reaction energy of the $2CO+O_2 \rightarrow 2CO_2$ reaction at both the PW91 and RPBE levels.

Structural relaxation is performed using the Broyden-Fletcher-Goldfarb-Shanno algorithm.[36] For identifying transition state (TS) configurations and a subsequent evaluation of reaction energy barriers, a constrained minimization technique is employed.[17] For each reaction, a relevant bond distance between the reactants is chosen as reaction coordinate and kept frozen at several values, while allowing the remaining degrees of freedom to relax. Then, TS is found when the energy reaches a maximum along the reaction coordinate, and a minimum with respect to the other degrees of freedom (as judged from a nearly zero atomic force). In the case of the more complex reactions (i.e., $CO+O_2$), a broad number of different relative orientations between the molecules are considered; this is found to be crucial in order to ensure the finding of the TS, as changes in orientation are observed to strongly influence the stability of the TS (more than 0.2 eV changes in several cases). In each case, care is taken that continuous reaction paths are indeed obtained, despite the use of a constrained relaxation search. This is done by plotting the potential energy along the reaction path as a function of the total change in the atomic coordinates (the change in the square root of the sum of all the Cartesian coordinates squared) rather than as a function of the constrained coordinate only.

TABLE I. PW91 and RPBE binding energies (in eV) for O_2, CO, and CO_2. For the latter, the heat of dissociation into CO and atomic O is given. The experimental values (quoted after the removal of zero-point energies) are taken from Ref. 35. Also given are the resulting reaction energies for the $2CO+O_2 \rightarrow 2CO_2$ reaction.

	PW91	RPBE	Expt.
O_2	5.88	5.53	5.23
CO	11.27	10.91	11.24
CO_2	6.32	5.99	5.63
$2CO+O_2 \rightarrow 2CO_2$	6.76	6.45	6.03

III. MORPHOLOGY OF Au PARTICLES ON MgO

Before undertaking the study of the reactivity towards CO oxidation, it is necessary to clarify in precisely which ways Au atoms and particles arrange themselves on the MgO(100) surface. Gas phase Au clusters have been characterized in great detail for small sizes, showing a tendency for planar structures up to 10—15 atoms.[37,38] At larger sizes 3D structures are preferred, with a preference for close-packed cub-octahedral, icosahedral, or decahedral shapes.[39] Recently, a very interesting tetrahedral shape linked to a closed-shell electronic structure has been found for Au_{20}.[40] Oxide-supported clusters are less well characterized, but some experimental studies of the structural features of nanosized Au clusters on MgO show that, in many cases, perfectly regular Au particles are able to grow epitaxially on the substrate, exposing a Au(100) facet at the top,[41–44] meaning that a Au(100)/MgO(100) interface is formed. The reason for this can be traced back to the rather small mismatch between the experimental lattice parameters of bulk Au (4.08 Å) and MgO (4.20 Å), meaning that only a 3% strain is necessary for the epitaxy to occur. With our theoretical approach, we reproduce this small mismatch with theoretical lattice param-

TABLE II. Adhesion potential energy and formation energy (both in eV) of several Au adsorbate structures on MgO(100). See Fig. 1 for sketches of each structure. The formation energies are given per atom in the Au system, whereas the adhesion potential energies are calculated per Au atom *in contact* with the substrate. The bulk Au cohesive energy per atom is shown for comparison. The Au-Au coordination number of Au in contact with the MgO surface is given for each system.

System	Au-Au coordination no.	Au layers	Adhesion energy RPBE (PW91)	Formation energy RPBE (PW91)
Au atom [a]	0	1	−0.56(−0.89)	−0.56(−0.89)
Au_2 [b]	1	2	−0.99(−1.36)	−1.54(−1.86)
Au_3 [b]	2	2	−0.44(−0.68)	−1.36(−1.74)
Au rod [a]	3	1	−0.05(−0.24)	−1.46(−1.90)
Au rod [b]	5	2	−0.16(−0.38)	−1.78(−2.30)
1 ML Au [a]	4	1	+0.01(−0.14)	−1.73(−2.20)
2 ML Au [b]	8	2	−0.14(−0.31)	−2.10(−2.67)
3 ML Au [b]	8	3	−0.12(−0.29)	−2.25(−2.83)
5 ML Au [b]	8	5	−0.10(−0.27)	−2.33(−2.93)
Bulk Au				−2.46(−3.08)

[a]All Au atoms at Au/MgO interface.
[b]Only some Au atoms at the Au/MgO interface.

eters of 4.22 Å (4.18 Å) for Au and 4.30 Å (4.25 Å) for MgO with the RPBE (PW91) XC description. We therefore choose in this paper to focus on the Au(100)/MgO(100) epitaxy.

A. The Au/MgO interface

We start by considering the properties of the Au/MgO interface, addressing the questions of the Au-MgO alignment at the interface and the energetics of the Au-MgO adhesion as a function of the Au coverage. In Table II we summarize the results obtained for the adhesion of a single Au atom, a Au_2 dimer, one-dimensional Au rods, and extended Au thin films to MgO(100). A two-layer-thick MgO slab was employed in the calculations, as we checked that an increase in the oxide slab thickness up to four layers, only leads to tiny changes (smaller than 0.01 eV) in the adhesion energies. For some of the systems considered, three locations of the Au atoms relative to the MgO(100) substrate were studied, with Au atoms either on top of oxygen or magnesium atoms, or at a hollow site. The results of this investigation are presented in Table III. In all cases studied, the O-top site is strongly favored. When constructing reasonable models for nm-sized Au clusters on MgO, Au atoms can therefore be assumed to be in registry with the oxygen atoms. Returning to Table II, several interesting effects are noticed. First, let us compare the two following types of systems: (a) absolutely *all* the Au atoms are in contact with the substrate and (b) other arrangements consist of *several* Au layers. The systems belonging to the (a) category appear much more weakly bound to MgO than those of the (b) category. This becomes apparent when comparing relatively analogous situations, i.e., a single Au atom and a Au_2 dimer oriented perpendicularly to the surface, a one-dimensional Au rod two atoms wide, either one or two layer thick, or an extended Au monolayer and layers two or more atoms thick. A beneficial effect is achieved when Au atoms are on top of the ones in contact with the substrate. As a consequence, 3D growth of Au on MgO is clearly favored, even for very small clusters. The presence of

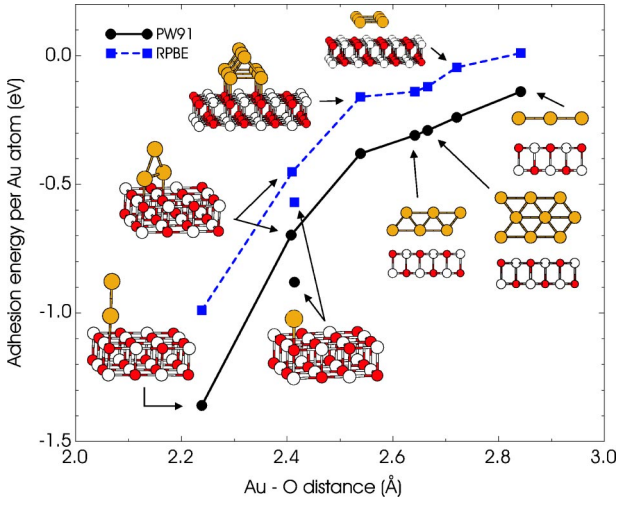

FIG. 1. (Color online) RPBE and PW91 adhesion potential energies as a function of the Au-O bond distance. Sketches show the different structures studied.

TABLE III. RPBE (PW91) adhesion potential energies for Au atoms or ML at several sites of the MgO(100) surface (in eV).

System	O top	Hollow	Mg top
Au atom	−0.57	−0.44	−0.31
	(−0.88)	(−0.72)	(−0.51)
1 ML Au	+0.01	+0.02	+0.02
	(−0.14)	(−0.12)	(−0.09)
2 ML Au	−0.14	−0.04	+0.02
	(−0.31)	(−0.17)	(−0.08)
3 ML Au	−0.12	−0.03	+0.07
	(−0.29)	(−0.17)	(−0.06)

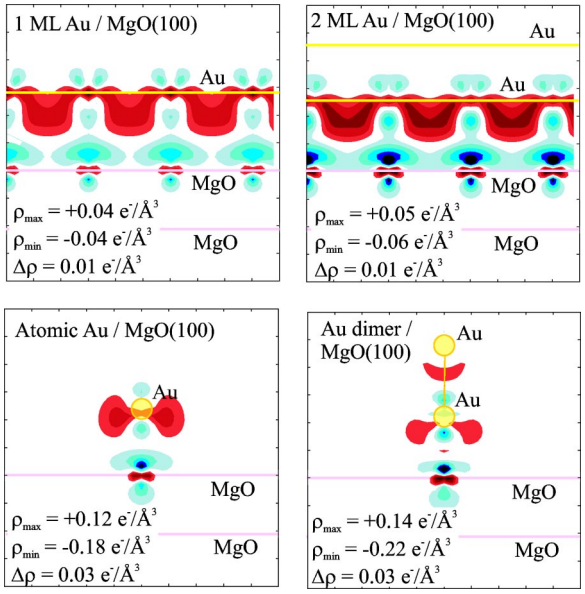

FIG. 2. (Color online) Induced charge densities (see text) for various continuous and discrete Au structures adsorbed on MgO. ρ_{max} and ρ_{min} denote the maximum and minimum charge-density differences, and $\Delta\rho$ the interval between contours.

this effect also indicates that the planar structures found for small free Au_n clusters ($n \lesssim 10$) (Refs. 38, 45 and 46) are likely to arrange perpendicular, and not parallel, to the MgO substrate when adsorbed over it. We have checked that this is indeed the case for Au_3, which binds in a perpendicular arrangement with two Au atoms on top of two substrate O atoms and the third Au atom on top of them, rather than as a flat lying triangle. Finally, let us note that this happens when substrate vacancies are absent: for TiO_2, indications point to preferred ''lying down'' configurations for very small Au clusters whenever vacancies are present.[47] The second effect is a general increase in adhesion as the Au-Au coordination of the Au atoms in contact with the substrate decreases. This statement does not, however, always apply: the binding enhancement due to having two-layered systems is always superposed to the coordination effect and can even overrule it. For example, an extended Au monolayer binds more weakly than a bilayer, although the coordination in the first case is 4 and in the second case 8. The same happens with Au_2 and Au_1, or with the (a) and (b) types of 1D Au rods. Comparing analogous situations with the same number of ''layers,'' however it is clear that less coordinated Au atoms bind more strongly to MgO. Finally, for extended Au overlayers the adhesion energy slowly decreases with the number of layers (leaving aside the anomalous case of 1 ML).

It is interesting to note that a direct correlation between the calculated adhesion energies and the Au-O equilibrium distance is found (see Fig. 1). Shorter Au-O bond distances result in a stronger Au-substrate binding. In order to study the origin of the adhesion between Au and MgO, and to clarify the strong changes that occur as the Au-Au coordination or number of Au layers vary, we plot in Fig. 2 the induced electron charge densities for several model systems. The induced charge densities are defined as the difference,

$$\varrho_{ind} = \varrho(\mathrm{Au/MgO}) - \varrho(\mathrm{Au}) - \varrho(\mathrm{MgO}),$$

between the charge density of the complete Au/MgO system and the ones for the Au and MgO subsystems. This difference is positive in the regions where the electronic charge accumulates upon formation of the complete system, and negative where the charge is depleted. The charge-density contours are shown for 1 ML Au, 2 ML Au, one free Au atom, and a Au_2 dimer. For an easier visualization, the 3D charge densities have been averaged along the *y* coordinate and plotted along *x* and *z*. A sizable charge transfer from the oxygen atoms in the first layer of the oxide to Au can be observed. Comparing 1 and 2 ML of gold, or 1 Au atom with a Au_2 dimer, it becomes clear that the presence of extra Au atoms above the contact region enhances the charge transfer, and consequently the adhesion. Also, a comparison of 1 ML Au with a single Au atom clearly shows that the magnitude of the charge transfer becomes larger as the coordination decreases, resulting again in a stronger binding.

Concluding the adhesion study, we note that the calculated adhesion potential energy is generally small, which is in agreement with a bonding mechanism based mainly on polarization and weak ionic bonding.[48,49] Using the most favorable value, -0.31 eV (or -0.55 J/m^2) per Au contact area (obtained for the 2 ML thin film at the PW91 level), this energy is clearly too moderate to cause 3D structures to spread over the support since this would simultaneously create more Au(100) surface which we calculate to cost 0.46 eV per Au atom (0.84 J/m^2). We must stress that these values must be taken as approximate, since systematic errors on calculating DFT surface energies may occur.[50,51] The ratio E_{adh} to E_{surf} is, however, expected to be reasonably correct. Our density-functional-theory calculations thus show, in agreement with experiments, that the growth of Au on MgO should occur in the form of 3D particles, and not as extended 2D structures.

B. Modeling Au/MgO interface boundaries

We now focus on the problem of modeling the Au-MgO interface boundary for nm-sized Au particles. In order to construct meaningful models, it is essential to discern how these particles arrange on MgO. The Wulff-Kaichew construction[52,53] provides some help for this, predicting the shape of large metal particles in thermodynamical equilibrium on a support in terms of a few parameters: the surface energy of the crystal facets and the metal-oxide adhesion energy. Also, in the case of particles surrounded by an atmosphere, the adsorption bond strength of molecules from the gas phase should be taken into account.[54] The Wulff-Kaichew construction translates the minimization of the (free) energy of the supported cluster into the geometrical prescription illustrated in Fig. 3. The clusters become polyhedral, exposing only low-index crystal facets. In the case of Au, packing requirements and the higher energy of the fcc(110) facet result in structures exposing only fcc(100) and fcc(111) facets.[55–57] The presence of the substrate results in a truncation of such polyhedra, with the degree of truncation determined by the metal-oxide adhesion energy.[58,59] The shape in Fig. 3(a) is derived using our theoretical values for

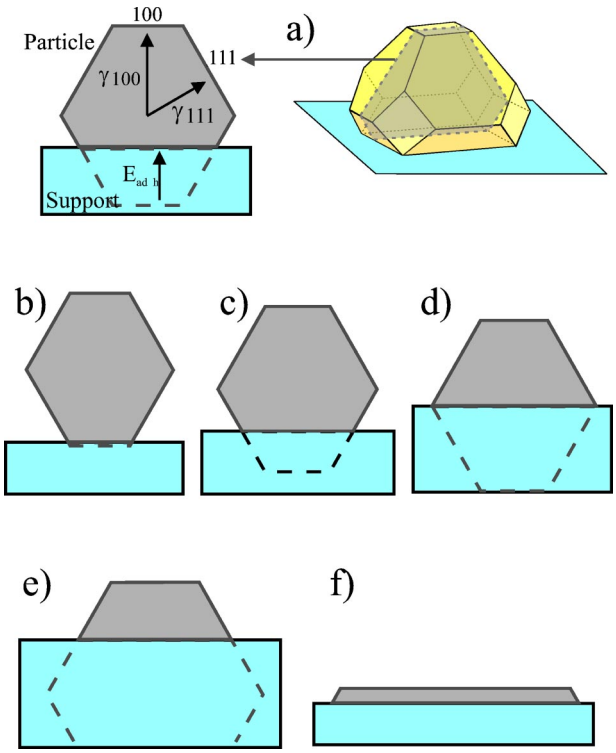

FIG. 3. (Color online) (a) Illustration of the Wulff-Kaichew construction. For all crystalline planes, vectors normal to the planes are plotted starting at the origin, having lengths proportional to the surface (free) energy of the planes (typically only low Miller index planes are relevant). At the apex of every vector a normal plane is plotted, and the polyhedron enclosed by these planes shows the equilibrium shape of the unsupported cluster. For the supported cluster the shape is derived by letting the vector normal to the interface plane be proportional to the surface energy of this plane *minus* the adhesion energy. (b)–(f) Truncated Wulff polyhedron in the case of (b) very small wetting ($E_{adh} \ll E_{surf}$); (c)–(e) increasing degree of wetting ($E_{adh}=0.5E_{surf}$, $E_{adh}=E_{surf}$, $E_{adh}=1.5E_{surf}$); (f) complete wetting ($E_{adh} \simeq 2E_{surf}$).

the surface energies and the adhesion energy. In Figs. 3(b)–3(f) we illustrate how the shape changes as the ratio between the surface energy and the adhesion energy changes. The larger the value of adhesion energy with respect to the surface energy of the interface facet, the larger the degree of truncation. When the adhesion energy equals the surface energy of the interface facet of the particle, the polyhedra are cut in half exactly (this is the limit of hemispherical shapes for supported liquid droplets). When the adhesion energy equals or exceeds the sum of the surface energies of the interface facet and the top facet, the limit of complete wetting, i.e., 2D growth, is reached.

TEM observations by Pauwels *et al.*[42] of Au nanoparticles on MgO indeed show the formation of truncated Wulff polyhedra similar to the sketch shown in Fig. 3(a). The authors, however, also provide evidence for the existence, at very small sizes (1–2 nm), of truncated pyramids with stronger wetting. This is not at all surprising, since for small particles the Wulff-Kaichew construction becomes uncertain: the extra contribution for the formation energies of edges and corners becomes important, as does the strain due to lattice mismatch

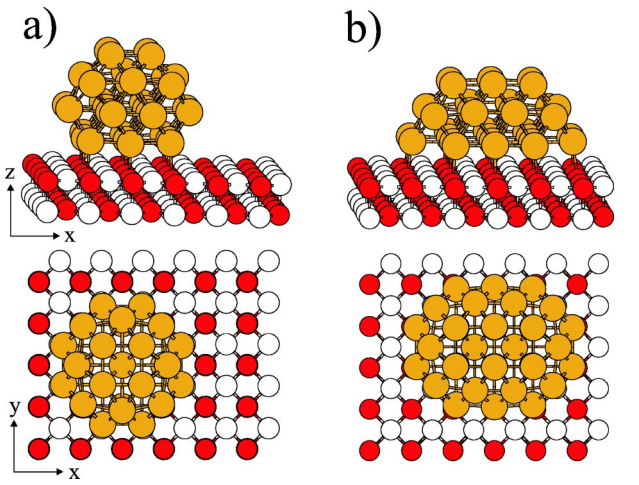

FIG. 4. (a) and (b) Top and side views of two relaxed isomers (calculated using DFT at the PW91 level) of Au_{34} supported on MgO(100), with different degrees of partial wetting.

between Au and the oxide, in the case of epitaxial growth. In this regime, alternative structures begin to compete with truncated Wulff polyhedra. For very small clusters (<50 atoms) it is possible (although computationally very demanding) to use DFT to compare the stability of competing cluster shapes. In Fig. 4 we present the relaxed structures of two different isomers of supported Au_{34}: (1) the truncated Wulff polyhedron [Fig. 4(a)], corresponding to the calculated E_{surf} to E_{adh} ratio, and (2) the alternative, truncated pyramidal cluster [Fig. 4(b)], which looks more like a truncated Wulff polyhedron with the $E_{surf}=E_{adh}$ relation. The first structure shows a smaller degree of wetting than the second structure. We find Au_{34} to be the ideal cluster size that allows for the construction of both types of structures without introduction of defects in any of them. The latter feature is particularly important, since it renders a direct comparison of the relative stabilities possible. In both cases, 2 ML of MgO with a $p(6\times5)$ unit cell are used as the substrate; this ensures a minimum cluster-cluster distance of 6 Å, large enough to make intercluster interactions negligible. The PW91 self-consistent results show that both arrangements have very similar stabilities, with the pyramidal one preferred by about 0.2 eV, thereby confirming a transition for very small sizes from truncated Wulff polyhedra conforming with the surface and adhesion energies to other structures, possibly with a larger degree of wetting. The same behavior has been demonstrated by semiempirical calculations for Pd clusters on MgO,[60] where the transition was observed to occur at $\approx$2 nm cluster diameter.

In order to gain insight into the reasons for this behavior, we have calculated the total energies of each isomer *without* the MgO substrate, in the frozen structure corresponding to the final relaxed configuration with the presence of the support. The truncated Wulff polyhedron is more stable by 1.55 eV than the truncated pyramid due to its more regular and rounded shape (sharp corners are energetically unfavorable, except in very particular cases, cf. Ref. 40). The evaluation of the respective adhesion energies to the support results in a much larger binding (−4.38 eV) to MgO for the pyramid

than for the truncated Wulff polyhedron (-2.72 eV) due to the larger contact area in the former case (16 atoms) than in the latter one (nine atoms). Such extra binding compensates for the intrinsic loss in structural stability, making the two structures almost equally stable. The non-self-consistent RPBE results differ slightly from the self-consistent PW91, favoring the truncated Wulff polyhedron by 0.35 eV due to a smaller value of the adhesion energies at the RPBE level (see Table II); the lack of extra stabilization provided by the larger contact area results in a preference for the intrinsically more stable shape. Leaving functional problems aside, the fundamental conclusion is that for these small sizes both types of shapes are extremely close in energy and are likely to appear.

Having realized that the shape of the Au clusters varies with the cluster size, the relative abundance of possible active sites on the facets and at edges and corners between facets obviously varies with the cluster size as well. More interesting, however, is the situation at the periphery of the Au-MgO interface region, where special types of sites appear for clusters in certain size ranges only. In modeling these sites, we shall not describe very large clusters since this would be too CPU demanding (the structural relaxation of the Au_{34} clusters above represents several weeks of eight parallel PC CPU's). Also, we shall not be using clusters of more limited sizes, since for these we expect corner and edge effects to dominate. Rather, we will describe the straight sections of the Au/MgO interface boundary of nm-sized particles by the infinite, straight boundaries between one-dimensional Au rods and the MgO support. These systems lend themselves to a representation in small periodic supercells as required already by our use of a plane-wave basis for the electronic states. In Fig. 5 the Au rod system is illustrated and the structures of the four specific interface boundary models, type I-IV, are shown. A $p(5\times2)$ MgO unit cell is used as support, large enough to avoid spurious interactions both in the x direction (due to interactions between the adsorbates at the interface and the back of the model Au rod) and in the y direction. We checked that by enlarging the unit cell of the type-II interface from $p(5\times2)$ to $p(5\times3)$ (three Au atoms per unit cell in y instead of two), the RPBE adsorption potential energy of a $CO\cdot O_2$ reaction intermediate (to be discussed later) changes only from -0.65 eV to -0.80 eV. From this, we judge that the finiteness of the unit cell will not affect the main conclusions of the study. The models reflect the different possibilities that are likely to appear as the cluster size increases. In the first place, terminations like the one labeled type I are expected for very small clusters with a large degree of wetting. At a given size, a transition should occur to the type-II interface, where an edge between two facets is in close proximity to the substrate. This edge is in what can be thought of as the ''equatorial plane'' of the Wulff polyhedron. Clusters of larger sizes will have metal-oxide interfaces, as characterized by the type-III interface, where the edge is located further from the surface. Since the Au edge for the type-III interface is far from the substrate, this edge represents a good approximation to other edges formed by the intersection of (111) facets around a large nanoparticle. Finally, we have explored another situation similar to the type-I case with a restricted cluster height of 2 Au monolayers; this case is labeled as type IV. According to the discussion above, the (equilibrium) formation of this type of interface would require a large adhesion energy compared to the surface energy, which could be achieved either through a high defect concentration in the oxide or through a large adsorption energy of adsorbates at the surface of the particle.

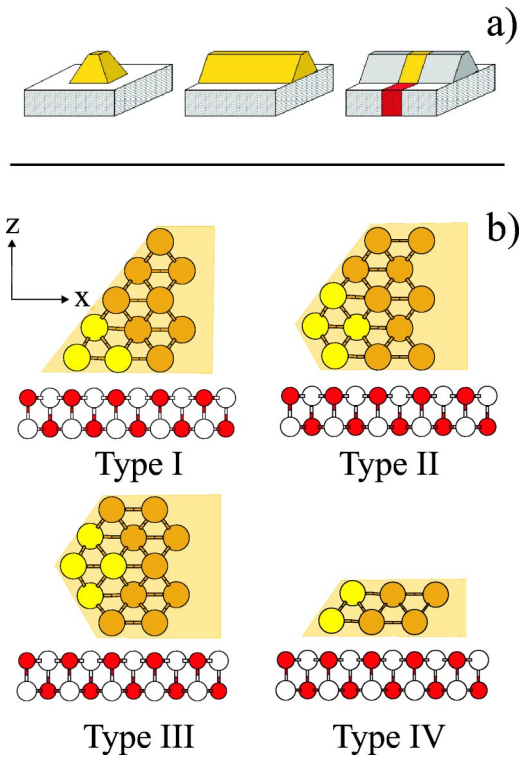

FIG. 5. (Color online) (a) Schematic illustration of the Au rods used in modeling different Au/MgO interface boundaries. (b) Ball and stick models of the four models considered.

The four systems in Fig. 5 represent most of the situations likely to be encountered in a regular Au particle supported on MgO. As we expect the general phenomena to be already present for these systems, we omit two other relevant cases: edges formed by an intersection of (111) and (100) facets at the top of the particle and the perpendicular intersection between a (100) facet and the MgO substrate. In all cases, some of the gold atoms around the edge (highlighted in the figure) are relaxed freely. The remaining atoms are kept frozen at the equilibrium positions they attain in a calculation where an extended five-layer slab on top of MgO is allowed to relax. The procedure is necessary as the small difference in lattice parameters between Au and MgO produces some changes in the Au interlayer distances. It must be stressed that the main drawback of the present approach is the neglect of describing corner sites. Although such sites are much less abundant (compared to edge sites) for a Au particle of ~2–3 nm diameter, they are nevertheless expected to have a sizable contribution to the overall particle reactivity, due to the low coordination. To gain some insight into the relative activities of corner and edge sites, we have simulated the adsorption of CO around a Au_{34} cluster. A somewhat simplified model,

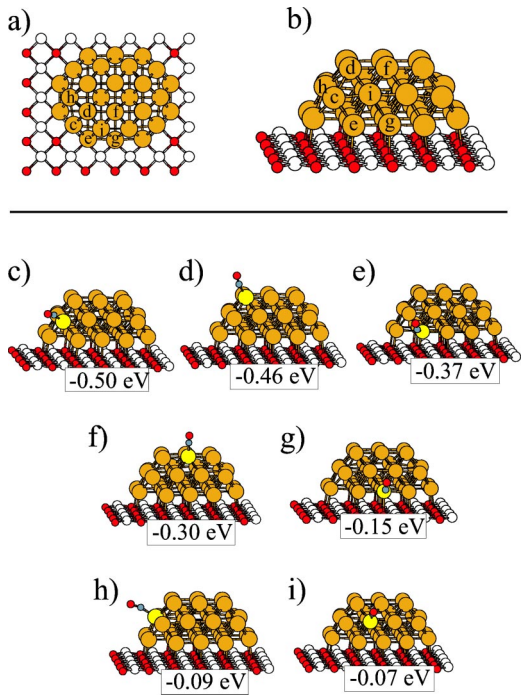

FIG. 6. (Color online) (a,b) Top and side views of a supported Au_{34} cluster, with labels marking several possible CO binding sites. (c–i) Relaxed structures and adsorption potential energies (in eV) for CO adsorption at Au_{34}; each panel is labeled by the corresponding site, defined in the upper panels.

with only one MgO layer as support, has been employed in order to reduce the high computational cost of these simulations. The results are shown in Fig. 6. A clear distinction is observed between the activity of corner (c–e), edge (f, g), and facet (h, i) sites, with larger CO binding energies for lower-coordinated sites. As corner sites are fairly active, we expect that an important part of a particle's reactivity can be attributed to its corners (but, as stated already, for computational reasons we focus in the remainder of this work on the reactivity of Au edges). Apart from the coordination effect, we also find in Fig. 6 a sizable decrease in the CO binding energy for sites in the first Au layer (e, g). We will show later that this behavior can be understood in terms of a steric repulsion of CO by the MgO support.

In order to compare the electronic structure of finite clusters and the extended 1D rods used in our work, we present in Fig. 7 the total and local densities of states (LDOS) for the two competing isomers of supported Au_{34}, as well as for two 1D extended rods with shapes matching the ones of the finite clusters. For an easier visualization, the LDOS' are averaged along the x and y direction, and plotted as isocontours depending on energy and the height z. In order to establish a direct comparison of the values of the DOS around the Fermi level, for each case the LDOS values are scaled by a factor related to the total number of electrons in the system, since the calculations for the different systems considered involve a variable number of atoms. As expected, the results show a slightly more conductive character for the supported rods than for the finite clusters. Also, it is interesting to note that the values of the DOS at the Fermi level are larger for sys-

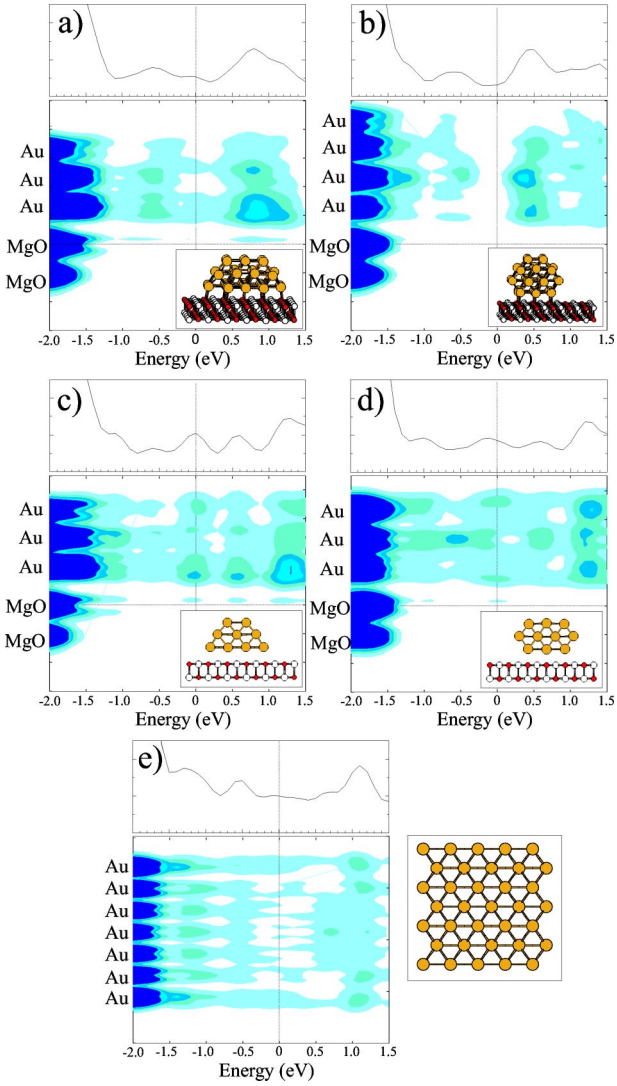

FIG. 7. (Color online) Local (lower panels) and total (upper panels) densities of states around the Fermi level (0 eV) for a supported Au_{34} cluster (a and b), one-dimensional Au rods (c and d), and Au slabs seven atoms thick (e). Labels in the y axis indicate the position of each atomic plane. See text for details.

tems (both clusters and rods) with a stronger degree of partial wetting. The moderate difference between finite clusters and 1D rods gives us confidence in the reliability of the present approach.

Finally, as mentioned in the Introduction, we will study the reactivity of Au(100) and Au(111) facets. In this case, we approximate finite cluster facets by extended Au slabs four layers thick (with the first two relaxed). Since these systems are not supported we use here the Au lattice constant, meaning that we model cluster facets without strain, which is the appropriate condition for large clusters.[61]

IV. CO OXIDATION REACTION

In this section we present the calculated adsorption and reaction configurations for O_2 and CO and related species along the reaction path for the catalytic oxidation of CO. We

will be working with the implicit assertion that a low adsorbate coverage situation is of relevance for the working catalyst. One adsorbate at a time is brought into contact with the various Au surfaces. At a first glance at the overall reaction,

$$CO + \tfrac{1}{2}O_2 \rightarrow CO_2,$$

it seems likely that the reaction will proceed as a Langmuir-Hinshelwood reaction with separate CO adsorption and dissociative O_2 adsorption steps, followed by CO+O recombination and CO_2 desorption steps:

$$O_2 \rightarrow 2O(a),$$

$$CO \rightarrow CO(a),$$

$$CO(a) + O(a) \rightarrow CO_2.$$

We will refer to this set of reaction steps as *pathway I*. As will become apparent below, our calculations support a slightly more elaborate set of reaction steps, *pathway II*, involving a $CO \cdot O_2$ reaction intermediate:

$$CO \rightarrow CO(a),$$

$$CO(a) + O_2 \rightarrow CO \cdot O_2(a),$$

$$CO \cdot O_2(a) \rightarrow CO_2 + O(a),$$

$$CO(a) + O(a) \rightarrow CO_2.$$

Each reaction step will be discussed in detail below.

A. Molecular and atomic oxygen bonding

Since the formation of surface oxides has been identified as an important factor in the catalytic activity towards CO oxidation on transition and noble metals,[62–66] we start out by investigating the adsorption of molecular and atomic oxygen at each of the several Au and Au/MgO systems considered. The special character of the low-coordinated sites at the edges of Au clusters makes the possibility of a high oxygen binding at those sites an interesting matter of consideration. The results, however, show that molecular O_2 binds very weakly to every type of edge site. In Fig. 8 we plot the most stable bonding configurations for O_2 at the type-I, -II, -III, and -IV interfaces. With small differences, in all the cases the self-consistent RPBE potential energies indicate an endothermic adsorption reaction, whereas the non-self-consistent PW91 data only show a weakly exothermic adsorption behavior (cf. Table IV). The same weak O_2 adsorption is found for both Au(100) and Au(111) facets and for 2 ML thin films of Au on MgO. Along with the weak adsorption energetics, we find O_2 adsorbed in a superoxo state, with its bond length enlarged from 1.24 Å (gas phase value) to ~1.35 Å, having a magnetic moment of $\sim 0.8\mu_B$. This is consistent with O_2 adsorption simulations for O_2 at Pt, where a similar superoxo state is found (now strongly bound), together with a peroxo-like state of similar stability and with a ~1.43 Å bond length and zero magnetic moment.[67,68]

The most stable configurations (and corresponding RPBE adsorption potential energies) for atomic oxygen adsorbed on type I-IV edges are shown in Fig. 9. The atomic oxygen shows a marked tendency to bind at low-coordinated edge sites. Binding energies at Au(100) or Au(111) facets are much smaller (see Table IV). A coordination effect clearly exists[11,12] that will be examined in further detail in the Analysis section. Besides, the atomic oxygen always prefers to attach at bridge sites between two Au atoms; only in the case of Au(100) facets hollow sites become competitive. In all cases, top sites are strongly unfavorable. O-binding site preferences at transition metals have been interpreted by Fei-

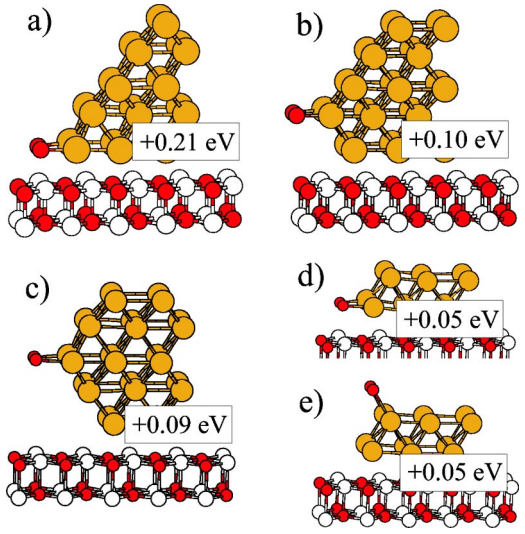

FIG. 8. (Color online) Lowest-energy arrangements and self-consistent RPBE adsorption potential energies of molecular O_2 at type I-IV edges.

TABLE IV. RPBE reaction energies (in eV) for molecular and dissociative O_2 binding at different types of edges and facets. PW91 results are shown in parentheses. In all cases, the energies are referred to O_2(g). The adsorption sites are described for most systems in Figs. 8 and 9. For Au(100) and Au(111), the adsorption sites are the bridge site for atomic O [with the hollow site rather close in energy for Au(100)] and a bridging site with the molecular axis parallel to the surface for molecular O_2.

	Type I	Type II	Type III	Type IV (a)
$O_2 \rightarrow O_2$(a)	+0.21 (−0.16)	+0.10 (−0.20)	+0.09 (−0.19)	+0.05 (−0.31)
	Type IV (b)	2 ML Au/MgO	Au(100)	Au(111)
	+0.05 (−0.18)	+0.22 +0.01	+0.13 (−0.02)	+0.11 (−0.01)
	Type I	Type II	Type III	Type IV (a)
$O_2 \rightarrow 2O$(a)	−0.29 (−0.77)	+0.19 (−0.40)	+0.71 (+0.28)	−0.82 (−1.26)
	Type IV (b)	2 ML Au/MgO	Au(100)	Au(111)
	+0.50 (+0.02)	+0.39 (−0.09)	+0.97 (+0.41)	+1.54 (+0.97)

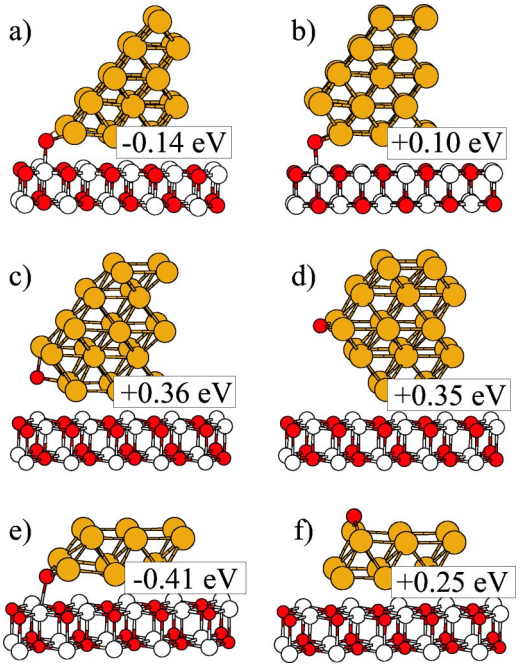

FIG. 9. (Color online) Self-consistent RPBE adsorption potential energies of atomic oxygen at several sites of type I-IV edges. The energies are calculated as $E_{\mathrm{ads}}=E(\mathrm{O/Au/MgO})-\frac{1}{2}E(\mathrm{O_2(g)})-E(\mathrm{Au/MgO})$.

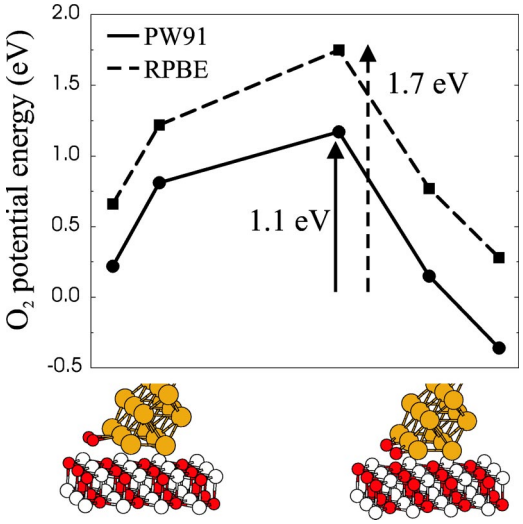

FIG. 10. (Color online) PW91 and RPBE potential-energy curves along the dissociation pathway for O_2 at the type-I interface. The sketches represent the initial and final states. The large difference (more than 0.5 eV) between RPBE or PW91 barriers (calculated with respect to gas phase O_2) reflects the great differences in the PW91 and RPBE descriptions of the O_2-Au binding. When the *intrinsic* activation energy for dissociation is calculated with respect to preadsorbed O_2, similar results are obtained with the two functionals.

belman in terms of an interplay between screening and interlayer bonds.[69] Let us highlight that, with very few exceptions, O_2 dissociation into adsorbed atomic oxygen is an endothermic process (in agreement with the nobleness of gold).[70] The exceptions are extremely interesting, as they always occur when oxygen is found at sites in direct contact with the substrate. In such cases [Figs. 9(a), 9(b), and 9(e)] oxygen binds to both low-coordinated Au atoms and a Mg substrate ion. The short O-Mg distance (2.2 Å, very close to the 2.15 Å O-Mg bond distance in bulk MgO) strongly suggests an O^{2-} electronic configuration for the adsorbed O atom. We will later analyze the origin of this effect. Finally, we must comment that the system formed by two Au monolayer thin film on MgO possesses some special features concerning the binding of atomic oxygen. The extremely thin character of the Au overlayer results in a sizable increase of atomic O binding with respect to a Au(100) surface. This fact can be attributed to several simultaneous effects: first, the epitaxial growth of extended Au layers expands the Au equilibrium lattice parameter by $\sim 2\%$ (i.e., the difference between Au and MgO), making the overlayers slightly more reactive. We have checked this point by performing additional calculations on a Au(100) surface modified by expanding the unit cell in the *x* and *y* directions in such a way as to match the lattice expansion for the Au/MgO system. The RPBE (PW91) adsorption potential energy of atomic oxygen changes from $+0.97$ eV ($+0.41$ eV) to $+0.83$ eV ($+0.27$ eV), i.e., in the direction of less endothermic reaction energetics. Other effects that must be responsible for the remaining binding enhancement are the reduced dimensionality of the overlayer and the possibility of adsorbate-oxide interactions through the Au film. The latter has been identified and analyzed for N adsorption at Pd films supported by MgO.[71]

B. O_2 dissociation

From the adsorption energetics of molecular and atomic oxygen adsorption just presented, it follows that although molecular O_2 does not easily bind to Au, its dissociation into atomically adsorbed oxygen can in some cases be energetically favorable. This, in principle, could represent the first stage of the CO oxidation reaction, as outlined above. In order to be kinetically feasible at low temperatures, the activation energy barrier for the O_2 dissociation must be low. Therefore, we have calculated the energy barrier for such process at a variety of configurations in the case of the type-I interface, a situation which shows a relatively strong binding of atomic oxygen. The results for the most favorable case (that is, the one with the lowest barrier) are presented in Fig. 10. The barrier is, even in this seemingly favorable case, rather large (more than 1 eV), and the relevance of processes involving direct splitting of O_2 will hence be low around room temperature. The TS is located at O-O bond distances around 2 Å. Also rather large barriers have been calculated by Yoon *et al.* for the O_2 dissociation at small unsupported Au clusters.[27]

Additional calculations for the dissociation of O_2 at a Au(100) surface show that the energetics of this reaction is very sensitive to the structural details. Placing molecular O_2 in a hollow site (see Fig. 11) and breaking it into two oxygen atoms at bridge sites results in an energy barrier (1.50 eV with RPBE, 0.95 with PW91) which is lower than that found

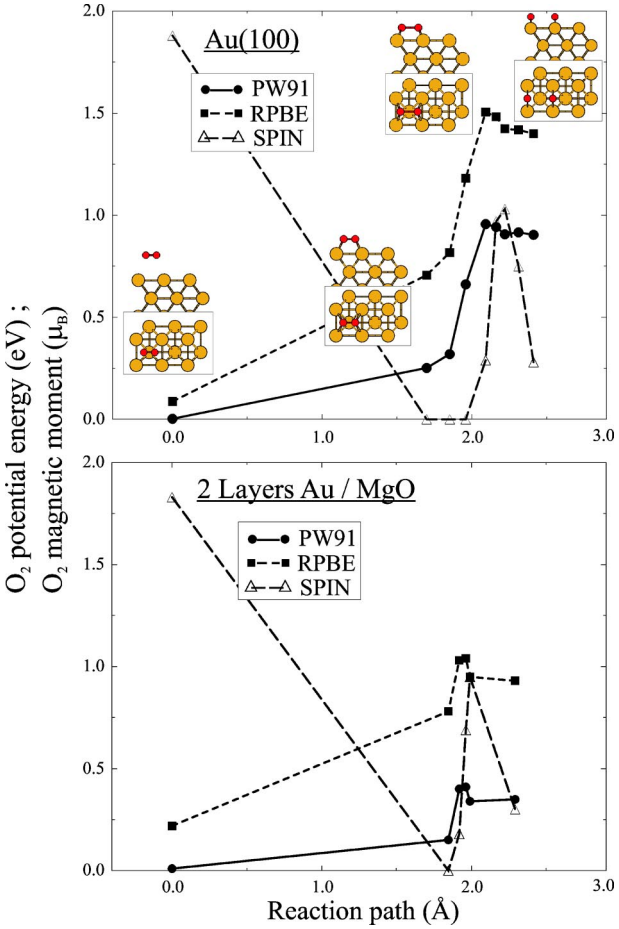

FIG. 11. (Color online) Reaction potential energy and spin for the dissociation of O_2 at a Au(100) surface and at two extended Au layers adsorbed on MgO. The sketches represent the various configurations along the path. The triangles represent the values of the magnetic moment for the O_2 molecule.

at the type-I interface. This is due to the relative proximity between two favorable bonding situations for both the initial (superoxo O_2^- molecule with each oxygen atom slightly bonded to two Au atoms in a near-bridge configuration) and final (each separate oxygen atom placed at a bridge site, the most stable location) states. It must be remarked that a noticeable difference between the binding energy of the final state and the one for two adsorbed oxygen atoms is seen, indicating a sizable O-O repulsion between the two coadsorbed oxygen atoms in the final state.

The potential-energy surface of O_2 along the reaction path shows some interesting features. At distances relatively far (>3 Å) from the surface, the O_2 properties resemble the ones of a free molecule, with an equilibrium bond length of 1.24 Å and a magnetic moment of $1.9\mu_B$. No sizable binding of O_2 to Au is found at this stage. As the molecule approaches the surface, it loses its magnetic moment and becomes trapped in a metastable superoxo O_2^- state with a bond length of 1.37 Å. Although the short O-Au distances (2.4 Å) indicate the presence of some binding (and its metastable character further confirms this), the disappearance of the magnetic moment reduces the overall binding energy,

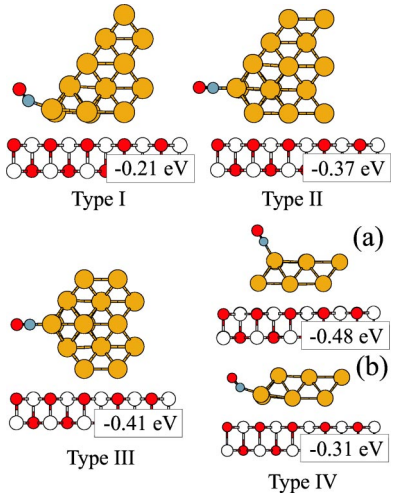

FIG. 12. (Color online) Most stable configurations of CO at the type I-IV interfaces, with the corresponding RPBE adsorption potential energies. For the type-IV case the upper (a) and lower (b) arrangements of CO are shown.

resulting in a nonbinding character of adsorbed O_2 in this configuration. From that point, the energy along the reaction path increases as the O-O bond distance is enlarged, and the TS state is found again at a distance of 1.9–2.0 Å. At this point we observe a quite striking behavior for the magnetic moment, which is quickly recovered at O-O distances around the transition state. This helps us to stabilize the TS and to lower the energy barrier for dissociation. A further enlargement of the O-O bond distance leads again to a decrease of the magnetic moment, which is nearly lost for the final state with two oxygen atoms bonded on neighboring bridge sites and separated 3.0 Å from each other.

In the case of the two Au monolayer films adsorbed on MgO, the low dimensionality of the system has the effect of substantially reducing the energy barriers to values between 0.5 and 1 eV (see Fig. 11). This is, we believe, the most interesting result, showing how finite-size effects may possibly increase the reactivity of a metal cluster. For our present purposes, modeling clusters of Au supported to MgO, we must, however, note that the thin Au film is an unlikely model, serving here only the purpose of a gedanken system. Also, we note that even with the relatively low barrier for O_2 dissociation, this Au system is not likely to show an overall high CO_2 formation along pathway I in comparison with what will be presented below for the type-II interface along pathway II. The deficiency of the monolayer film stems from a slightly endothermic O_2 dissociation and a weak adsorption of CO on the film.

C. CO bonding

The binding of CO at Au edges shows a very different behavior from the one calculated for O_2. In Fig. 12 we show the relaxed configurations for each of the Au edges under study. The corresponding adsorption potential energies are reported in Table V. In the case of the type-II, -III, and -IV interfaces, we obtain fairly large CO-Au binding energies of

TABLE V. RPBE and PW91 adsorption potential energies of CO (in eV).

	Type I	Type II	Type III	Type IV (a)
RPBE	−0.21	−0.37	−0.41	−0.48
PW91	(−0.50)	(−0.69)	(−0.72)	−0.80
	Type IV (b)	2 ML Au/MgO	Au(100)	Au(111)
RPBE	−0.31	−0.21	−0.21	+0.02
PW91	(−0.61)	(−0.62)	(−0.60)	(−0.26)

about 0.4 eV on top of Au atoms at the edge. CO shows a marked tendency to bind in the ''equatorial plane'' relative to the Au edge, and any inclination out of this plane leads to a sizable loss of stability. On the contrary, CO is found to diffuse very easily along the edges, with binding energies only marginally smaller at Au-Au bridge sites. In contrast, for very small Au clusters a clearer preference for top sites has been found,[72] but of course in this latter case corner effects are expected to dominate (cf. Fig. 6). CO binds at the type-IV edge [configuration (a)] slightly more strongly than at type-II or -III edges. This is probably due to the same low-dimensional effect that makes adsorbates bind more strongly to 2 ML Au/MgO than to a Au(100) surface. The binding of CO at Au(100) or Au(111) facets, or 2 ML Au/MgO, is much weaker than at the edges. CO therefore is expected under reaction conditions to be strongly concentrated at the edges (and corners) of Au nanoparticles. Incidentally, we have checked that the binding of CO at the MgO substrate can be neglected, with only −0.13 eV (PW91) and +0.05 eV (RPBE) adsorption potential energies on top of a Mg atom (the most stable site). The significant binding at low-coordinated Au atoms agrees well with experimental evidence for edge atoms as the only active sites available to CO adsorption on titania-supported Au clusters.[73] Nevertheless the values obtained are moderate enough to consider that, at room temperature, CO will reversibly adsorb at those sites. Low CO desorption temperatures have been measured on small supported Au particles by Shaikhutdinov *et al.*,[74] who also note that adsorption of CO exhibits a size effect in that small particles adsorb CO more strongly. Finally, the situation at the type-I and type-IV edges [conformer (b)] deserves special attention. In this case, CO shows an anomalous low binding of 0.2–0.3 eV and attains a bent configuration. This finding has important implications for the reactivity of type-I interfaces: as both CO and O_2 bindings are weak, the production of CO_2 based on pathway II will be strongly hindered, as the first stage of the reaction (CO binding) is difficult to attain. For the type-IV case, this is not so dramatic, as the possibility of strong CO bonding exists in the upper configuration.

D. CO+O_2 reaction

As we have already seen that CO is able to bind at low-coordinated Au sites, from now on we will focus on the study of CO_2 formation following pathway II, along which an adsorbed CO molecule reacts directly with an O_2 from the gas phase. Starting from the most stable configuration for CO in each case, we have simulated the approach and bonding of molecular O_2 to CO for all systems under study [type I-IV edges, Au(100) and Au(111) facets, and 2 ML Au/MgO]. The energetics for the reaction are shown in Fig. 13 (see Table VI for numerical values). The reaction proceeds in several stages. First, the reaction of O_2 with adsorbed CO leads to the formation of a rather stable $CO \cdot O_2$ reaction intermediate. In Fig. 14 we plot the most stable configura-

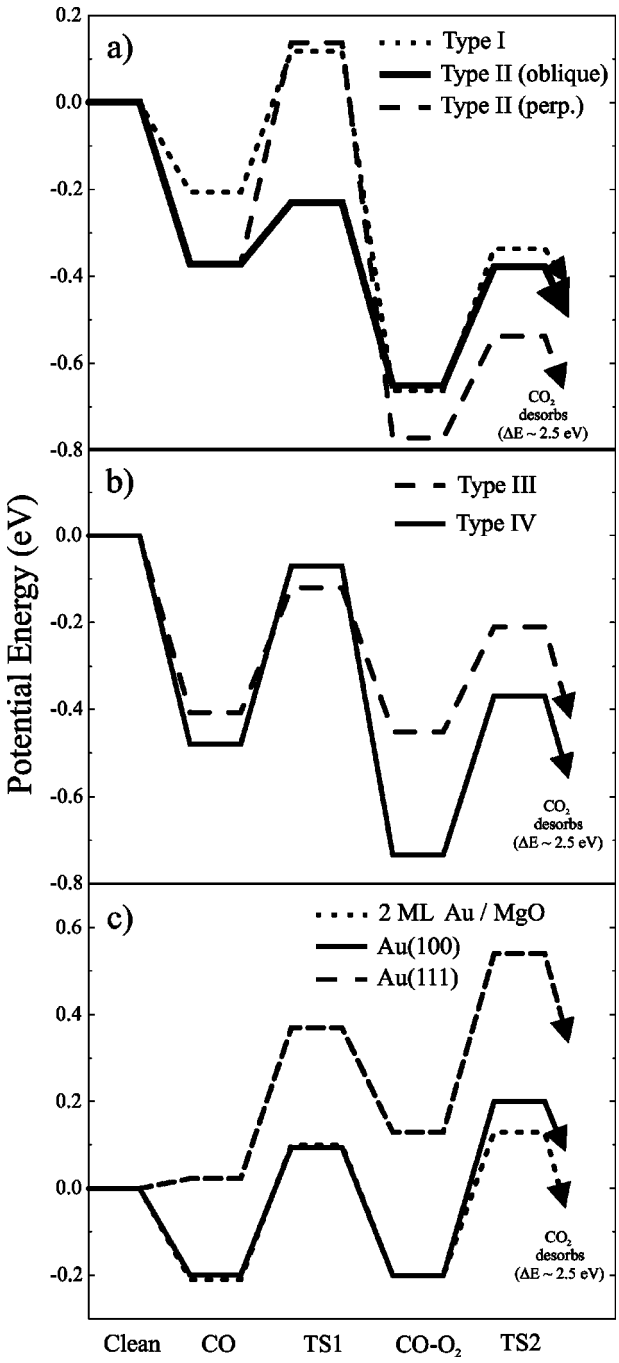

FIG. 13. RPBE reaction energetics for the CO+O_2→CO_2+O(a) reaction. (a) Type I-II Au/MgO interfaces; (b) type III-IV Au/MgO interfaces; (c) Au(111) and Au(100) facets and 2 ML Au/MgO.

TABLE VI. Reaction energies ΔE and activation energies E_a for the two stages of the $CO(a)+O_2(g)\rightarrow CO_2+O(a)$ reaction, calculated at the RPBE and (PW91) levels (in eV).

$CO(a)+O_2\rightarrow CO\cdot O_2(a)$				
	Type I	Type II [a]	Type II [b]	Type III
ΔE	−0.46	−0.40	−0.28	−0.04
	(−1.01)	(−0.99)	(−0.83)	(−0.46)
E_a	0.32	0.50	0.14	0.28
	(−0.14)	(0.07)	(−0.14)	(−0.01)
	Type IV	2 ML Au/MgO	Au(100)	Au(111)
ΔE	−0.25	−0.01	0.00	+0.11
	(−0.71)	(−0.47)	(−0.47)	(−0.43)
E_a	0.41	0.29	0.29	0.35
	(0.10)	(0.00)	(0.02)	(0.03)
$CO\cdot O_2(a)\rightarrow CO_2+O(a)$				
	Type I	Type II [a]	Type II [b]	Type III
ΔE	−2.69	−2.57	−2.45	−2.40
	(−2.27)	(−2.20)	(−2.04)	(−2.06)
E_a	0.33	0.23	0.27	0.24
	(0.34)	(0.28)	(0.28)	(0.17)
	Type IV	2 ML Au/MgO	Au(100)	Au(111)
ΔE	−2.87	−2.70	−2.51	−2.56
	(−2.48)	(−2.26)	(−2.21)	(−2.21)
E_a	0.37	0.33	0.40	0.41
	(0.38)	(0.35)	(0.40)	(0.39)

[a]Perpendicular conformer [Fig. 14(b)].
[b]Oblique conformer [Fig. 14(c)].

tions of this complex at the four different Au-MgO interfaces. It is noteworthy that for the type-II interface two possible conformations with comparable stabilities exist, one completely perpendicular to the edge (and slightly more stable) and another at an oblique orientation with respect to

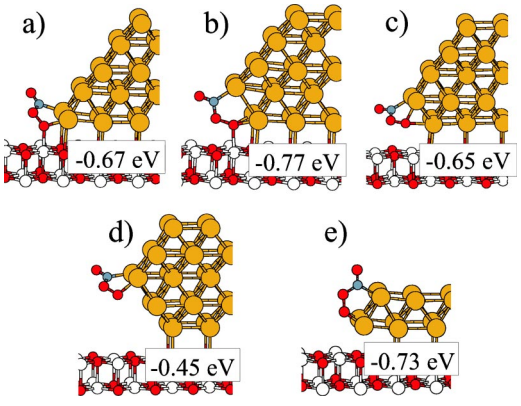

FIG. 14. (Color online) $CO\cdot O_2$ relaxed structures at (a) the type-I, (b) type-II (perpendicular conformer), (c) type-II (oblique conformer), (d) type-III, and (e) type-IV interface boundaries. For each structure the corresponding RPBE potential energy [calculated with respect to CO(g) and O_2(g)] is given.

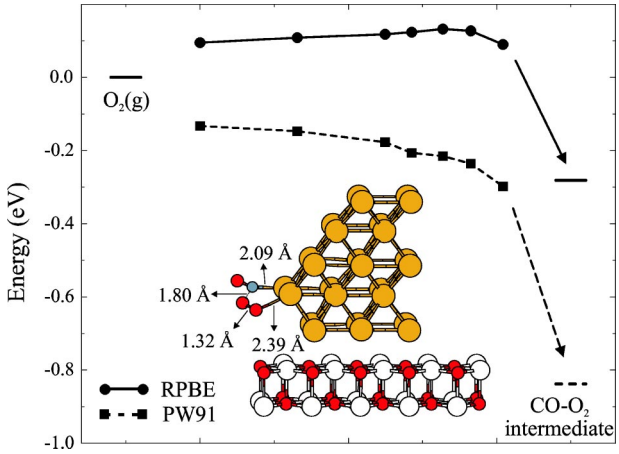

FIG. 15. (Color online) Potential energy along the reaction coordinate for the formation of $CO\cdot O_2$ at the type-II interface in the oblique orientation. The inset shows the structure at the transition state, indicating relevant interatomic distances.

the edge. This $CO\cdot O_2$ intermediate is characterized by ~120° O-C-O and O-C-Au angles and an O-O peroxo bond of about 1.45 Å (and zero magnetic moment). From a chemical point of view, the formation of the complex involves two major changes: (1) the transformation of the triple C-O bond in CO to a double bond, accompanied by the formation of a strong single bond between CO and O_2, and (2) the change from a double O-O bond in O_2 to a peroxo bond, together with the formation of a strong O-Au single bond. The finding that $CO\cdot O_2$ forms as a reaction intermediate is in accord with the identification of this very complex by vibrational spectroscopy for the $CO+O_2$ reaction on gas phase Au monomers at very low temperatures,[75] with the observation of cooperative CO and O_2 adsorption on various anionic Au clusters,[76,77] and with recent density-functional theory calculations.[78]

The most remarkable fact about the formation of the $CO\cdot O_2$ reaction intermediates is the very low-energy barriers involved. Only $CO\cdot O_2$ at either the type-II interface in a perpendicular orientation (0.5 eV) or at the type-IV interface (0.4 eV) is slightly more difficult to form, with RPBE activation energies of the order of 0.2–0.3 eV for the rest of the interfaces (only 0.14 eV in the oblique configuration at the type-II interface). It is also remarkable that in most cases the non-self-consistent PW91 results provide *negative* activation energies based on the RPBE-derived transition states, meaning that at the PW91 level the process is not activated, and O_2 can even bind to CO without having to overcome any barrier. This shows a marked tendency of CO bonded to Au to incorporate O_2 and to form the $CO\cdot O_2$ intermediate. Figure 15 shows the potential energy (RPBE and PW91) along the reaction path for the formation of $CO\cdot O_2$ in its oblique configuration at the type-II interface. The energy reference is taken as the total energy of the interface with CO adsorbed and O_2 in the gas phase. The potential-energy surface is very flat up to a point past the transition state, where the OC-OO single bond is formed and the energy suddenly decreases as

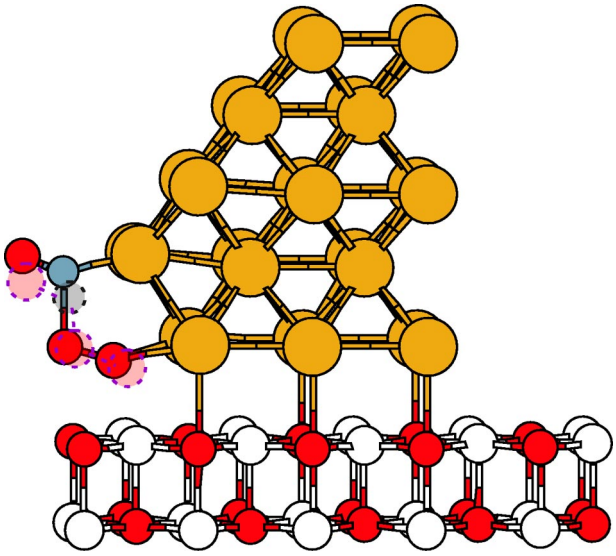

FIG. 16. (Color online) Structure of the transition state for the formation of $CO \cdot O_2$ at the type-II interface, in its perpendicular orientation. The structure of the final-state configuration is sketched as dashed circles.

the $CO \cdot O_2$ intermediate is formed. As just mentioned, no TS is found at the PW91 level, with $CO \cdot O_2$ being formed smoothly from gas phase O_2.

The larger value of the energy barrier to form $CO \cdot O_2$ in its perpendicular configuration at the type-II interface can be rationalized in terms of a too close distance in the TS of the O_2 and the MgO substrate (see Fig. 16). It is important to stress that molecular O_2 by itself does not bind to MgO; we calculate (PW91 self-consistent) an equilibrium height of 3.15 Å above the surface (in the absence of Au) with a very weak physisorption minimum ($+0.02$ eV with RPBE, -0.04 eV using PW91). In the configuration shown in Fig. 16, the lower oxygen atom in O_2 is located 2.26 Å above the surface, which is energetically unfavorable. The effect is completely reversed once the O_2 is part of a $CO \cdot O_2$ intermediate, in which case (as we show below) a fairly strong attractive interaction to the substrate occurs. We have explored the possibility of the perpendicular orientation of the $CO \cdot O_2$ intermediate to be formed by a rotation of the preformed intermediate in its oblique configuration (see Fig. 14), instead of direct bonding of gas phase O_2 to adsorbed CO. The results show the presence of a rather high-energy barrier (larger than 0.5 eV) for the O_2 capture via the rotation pathway. The large barrier builds up because the rotation involves the breaking of the strong bond between the terminal oxygen atom in $CO \cdot O_2$ and a bridge site between two Au atoms; in the TS that terminal oxygen atom is placed on top of a Au atom, which is not a very stable location (as seen before, either atomic oxygen or terminal oxygen atoms in $CO \cdot O_2$ intermediates strongly prefer to bind at bridging sites). Therefore, it can be concluded that although a remarkably stable perpendicular configuration can be formed at the type-II interface, the special geometrical features of the system prohibit its formation and leave the formation of the (also relatively stable) oblique configuration more likely to occur.

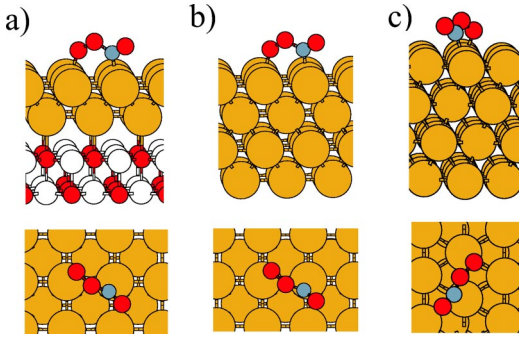

FIG. 17. (Color online) Side and top views of $CO \cdot O_2$ relaxed structures at (a) 2 ML Au/MgO, (b) Au(100), and (c) Au(111) surfaces.

The structures and the relative stabilities of the $CO \cdot O_2$ complexes vary strongly with the structure of the Au-MgO interface. For the I and II cases, the complex binds very near to the MgO support with an enhanced binding between 0.3 and 0.4 eV larger than the binding of CO alone. On the contrary, on interface III the $CO \cdot O_2$-MgO distance increases, and a sizable decrease of the stability of the intermediate occurs. In this latter case the reaction $CO(a) + O_2 \rightarrow CO \cdot O_2(a)$ becomes nearly thermoneutral. The reaction energetics at the type-IV interface boundary shows both large CO and $CO \cdot O_2$ stability, but here a sizable barrier is present for the $CO \cdot O_2$ formation. Altogether, reaction through the oblique $CO \cdot O_2$ conformer at interface type II [thick full line in Fig. 13(a)] appears to constitute the most favorable reaction path. We return to the cause of this in the Analysis section.

Moving to the $CO \cdot O_2$ formation at the planar Au facets, we show in Fig. 13(c) the reaction energetics for the three extended systems under study: 2 ML Au on MgO, Au(100), and Au(111). The reaction appears to be able to proceed without particularly high barriers, but in comparison with the interface systems considered above we note two effects that will effectively hinder a high reactivity of the planar systems: first, CO shows a rather weak binding and, second, the formation of the $CO \cdot O_2$ intermediate (see structures in Fig. 17) is a thermoneutral or slightly endothermic process. Two Au monolayers on MgO show a slight enhancement of the binding with respect to the Au(100) case, but the overall picture is the same. We therefore conclude that in the case of thin 2D Au clusters adsorbed on MgO, only the Au/MgO interface boundary would seem to be able to catalyze the reaction.

The last stage of the reaction involves the breaking of the $CO \cdot O_2$ intermediate into CO_2 and atomic oxygen left behind adsorbed in the Au particle. The energy barrier for this reaction is fairly constant for all systems studied, and amounts to around 0.3–0.4 eV [see Fig. 18 for TS structure and energies in the type-II (oblique) case]. The TS is found for an OCO-O bond distance of about 1.7 Å. This is not at all surprising, since this barrier is strongly related to the intrinsic properties of the peroxo O-O bond within the $CO \cdot O_2$ complex. The unstable character of the peroxo O-O bond makes the $CO \cdot O_2$ intermediate work as a ''trapping state,'' since once

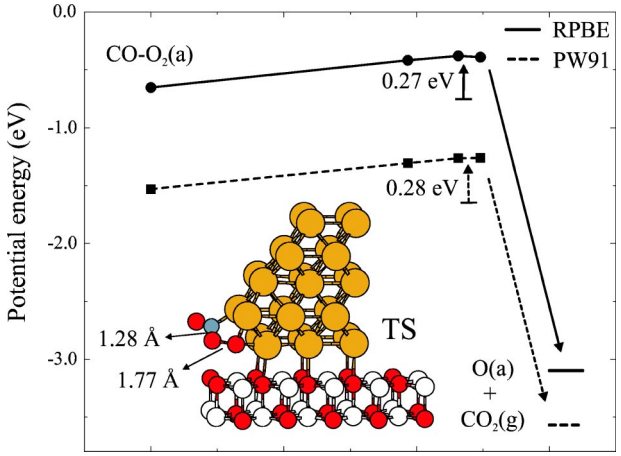

FIG. 18. (Color online) Potential energy along the reaction path (in eV, referred to gas phase CO and O_2) and view of the structure at the transition state (with some relevant bond distances indicated), for the breaking of the $CO \cdot O_2$ intermediate into CO_2 and atomic oxygen at the type-II interface (oblique conformer).

the complex is formed the only way out of it is the dissociation into CO_2 and O(a). These reasons support the idea of the rate-limiting step in the reaction to be the capture of O_2 by CO. After overcoming the moderate energy barrier, the CO_2 part of the intermediate quickly distorts to the linear shape of the free CO_2 molecule, breaking at the same time the C-Au bond. CO_2 immediately desorbs with an energy release of about 2.5–3 eV, depending on the Au/MgO system at which the reaction takes place.

E. CO+O(a) reaction

In order to complete the study of the catalytic cycle possibly performed by Au clusters, it is important to ensure that atomic oxygen left behind after the reaction between CO and molecular O_2 does not pollute the active sites. Therefore, we have studied in detail the reaction between adsorbed atomic oxygen and CO, in a variety of environments. Figure 19(a) shows the pathway involving the lowest-energy barrier for the reaction at the type-I interface. Trying different orientations of CO relative to O for the initial state (at a neighboring edge site and at a neighboring facet site, being preadsorbed on top of a Mg atom in the substrate, or coming directly from the gas phase), we find the latter possibility to be the preferred one. The smallness of the barrier (0.30 eV using RPBE or 0.05 eV using PW91) means that any atomically adsorbed oxygen can readily be reacted off by CO from the gas phase, thereby closing the catalytic cycle.

The type-II interface constitutes a very interesting case. The rather hidden location of the adsorbed O atom could, in principle, be considered as an obstacle for its detachment. The situation however is exactly the contrary. The calculated binding energy of CO to a Au edge site *exactly on top of the adsorbed O* is actually slightly larger (-0.41 eV with RPBE and -0.74 eV employing PW91) than the corresponding binding energy at a completely clean edge. Oxygen-covered edges therefore to some extent work as attractors for CO. Furthermore, calculations for the reaction between a pread-

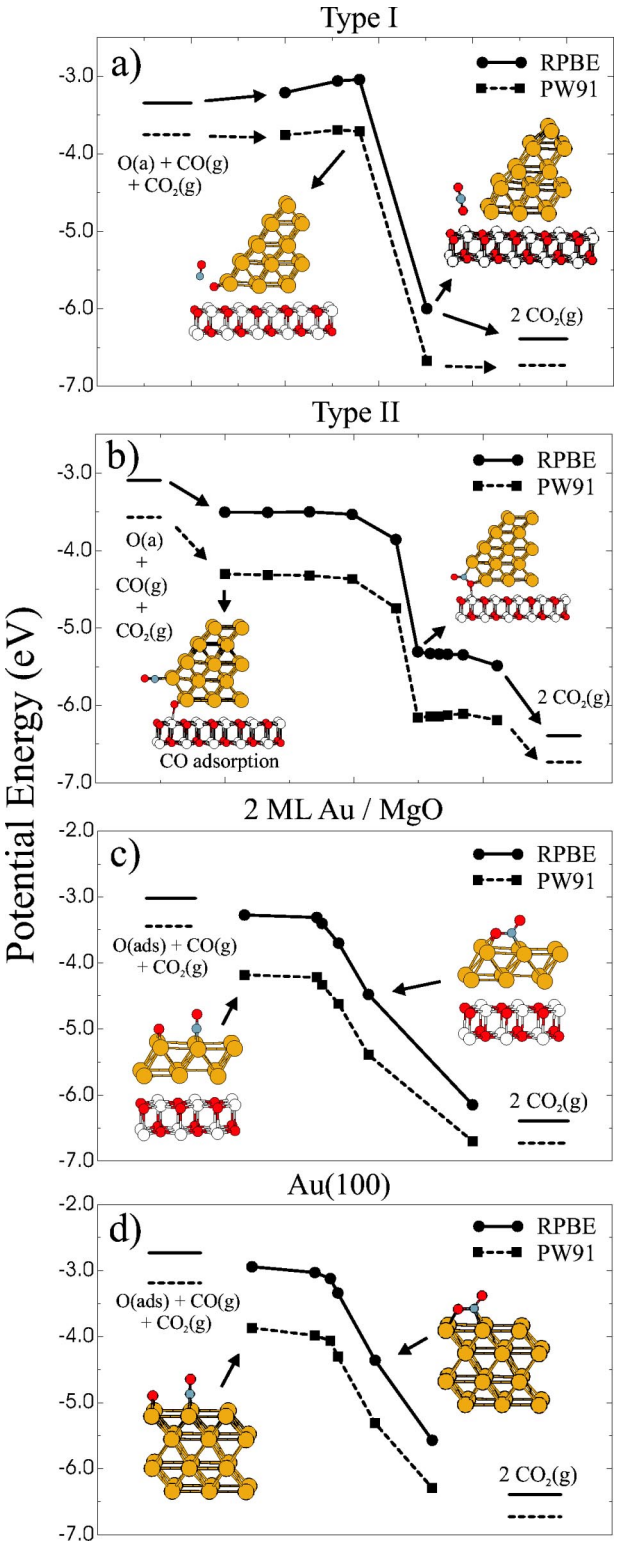

FIG. 19. (Color online) Reaction energetics and paths for the reaction between CO and the atomic oxygen left after the reaction between CO and molecular O_2, for (a) type-I and (b) type-II interfaces, and for (c) 2 ML Au on MgO and (d) Au(100) surfaces. The potential energy is calculated with respect to 2 CO and O_2 in the gas phase.

sorbed CO and O show that the CO molecule easily distorts from its location at the equatorial plane and binds to O, *without any distinguishable barrier*. After the formation of the OC-O bond, the CO_2 molecule becomes ''trapped'' at a nearly metastable state [see Fig. 19(b)] strongly resembling the perpendicular configuration of the $CO \cdot O_2$ intermediate at the type-II interface (but one oxygen atom short). Nevertheless, such a state is calculated to be 0.8 eV less stable than the free CO_2 molecule, and desorption is therefore expected to take place without difficulty. In fact, the calculated relaxation pattern obtained for a CO_2 molecule shows a tendency towards desorption after passing through an extremely flat potential-energy surface region.

Similar calculations performed on either the 2 ML Au on MgO or the Au(100) surface also indicate a very reactive character of adsorbed atomic oxygen that can be very easily removed by an incoming CO molecule [see Figs. 19(c,d)]. In both cases, CO can adsorb at a bridge site in the vicinity of the preadsorbed O, with binding energies very close to the ones associated to adsorption at an originally clean surface. Afterwards, as CO and O approach each other, the energy steadily decreases with the formation of CO_2 without the buildup of any energy barrier. Along such a pathway the CO changes its orientation progressively and in the intermediate stages of the reaction a $CO \cdot O$ complex is being formed, characterized by $\sim 120°$ angles and analogous to the one appearing at the type-II interface. The main difference with respect to this case is that now the pseudometastability is absent, and the complex [whose formation from $CO_2(g)$ is more endothermic than for the type-II interface] readily desorbs into $CO_2(g)$. This fact indicates a much less reactive character of either Au(100) faces or thin Au layers on MgO than for the type-II interfaces.

It is worth noting the similarities between the net reactions $CO + O_2 \rightarrow CO_2 + O(a)$ and $CO + O(a) \rightarrow CO_2$. In both cases CO attains an additional oxygen atom and transforms to CO_2 in two stages (see Fig. 20): first, a single bond is formed between carbon and oxygen; at this stage the carbon atom changes its hybridization from sp to sp^2, forming a double bond with one oxygen atom and another single bond with Au. The result is the formation of either $CO \cdot O_2$ or $CO \cdot O$ intermediates with varying stabilities depending on the environment. In the second stage, the attachment of O to CO is completed, with a change from a single to a double bond. This phenomenon occurs simultaneously with the breaking of the C-Au bond, the breaking of either the O-O or O-Au bond, and the transformation of the bent O=C—O group into the linear geometry of the free CO_2 molecule. Although the energetics strongly vary with the type of system considered, we can very roughly estimate the energy gain associated with the first stage (formation of the single C-O bond and an intermediate complex) to be of the order of 1 eV, whereas the completion of the reaction with formation of CO_2 in general represents an energy gain of around 2 eV. These estimates seem to hold (with a notable scattering, as we have just mentioned) for both $CO(ads) + O_2(g)$ and $CO(ads) + O(ads)$ reactions.

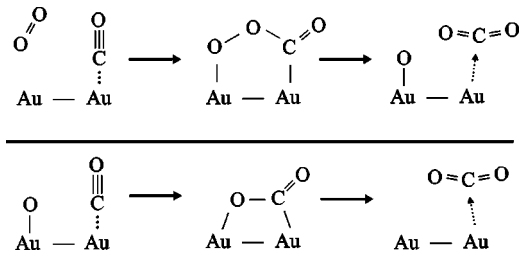

FIG. 20. Schematic representation of the reactions $CO(a) + O_2(g) \rightarrow CO_2(g) + O(a)$ (upper panel) and $CO(a) + O(a) \rightarrow CO_2(g)$ (lower panel).

V. ANALYSIS

In this section we will focus on the analysis of the results obtained for the type I-IV interfaces, and on the qualitative differences between them. More specifically, we are interested in discerning the physical origin of, first, the anomalously low binding of CO at type-I and type-IV interfaces (lower configuration) and, second, the enhanced stability of the $CO \cdot O_2$ intermediate at type-I, -II, and -IV interfaces, but absent at the type-III interface. Besides, we will also discuss the important effect of Au coordination on the reactivity of the different systems. Finally, another interesting issue to be investigated is the strikingly low value (0.14 eV) of the energy barrier leading to the formation of the $CO \cdot O_2$ intermediate at the type-II interface (in its oblique conformer).

A. CO anomalous low binding for type-I and type-IV interfaces

We start with the calculated lower binding of CO to type I and type IV compared to type-II and -III interface boundaries. From a mere Au-Au coordination point of view, the type-I Au atoms ought to be more reactive than the type-II and -III Au atoms, since for type I the Au atoms are only fivefold coordinated while they are at least sevenfold coordinated in the other cases. It turns out, however, that the Au atoms at a sharp edge in direct contact with the substrate are the least reactive towards CO adsorption. The influences of the presence of the substrate may be studied by performing calculations for CO binding at *unsupported* type-I or type-IV clusters. In the case of the type-I cluster, removing the MgO support, keeping the equilibrium orientation of CO at the supported edge, results in a negligible gain in binding energy of 0.01 eV [see Fig. 21(a)]. When the substrate is absent however such a configuration is no longer stable, but spontaneously relaxes to the arrangement depicted in Fig. 21(b). The relaxation leads to a further 0.20 eV stabilization, with a final CO adsorption potential energy of -0.41 eV. As expected, CO is placed again at the equatorial plane between the two facets intersecting at the edge. We therefore conclude that the anomalously low CO binding at the type-I interface is simply due to a sterical repulsion of CO by the substrate, which forbids CO to attain its most stable arrangement relative to the edge. Once the (hypothetical) optimal configuration of CO is realized by removing the substrate, the binding strength of CO becomes comparable to that at the type-II or

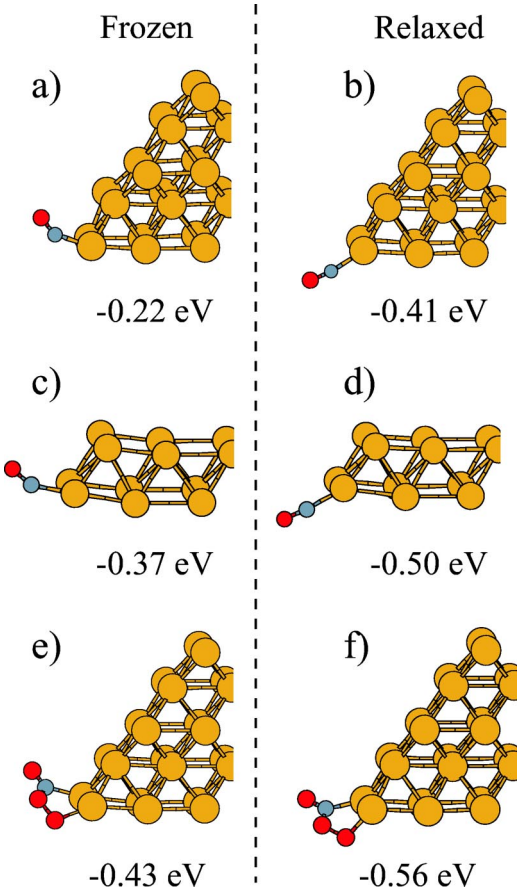

FIG. 21. (Color online) Frozen (a) and relaxed (b) configurations and potential energies of CO around an unsupported type-I edge. The same for CO at the type-IV edge (c, d) and for the CO $\cdot O_2$ reaction intermediate at the type-I edge (e, f).

-III interfaces. The same effect is observed for CO at the type-IV edge also [see Figs. 21(c,d)]; rotation of CO around the edge again leads to an improved binding. More strikingly, the same behavior can also be seen for the $CO \cdot O_2$ intermediate bonded at the type-I edge [see Figs. 21(e,f)]. In this latter case, however, the effect is completely masked by the attractive interaction between the reaction intermediate and the substrate (to be analyzed in the following section), and the net effect of the presence of the substrate is now an enhancement (by around 0.2 eV) of the stability of the intermediate.

B. Oxygen-MgO attractive binding

The $CO \cdot O_2$ configurations for the type-I and-II interface boundaries [see Figs. 14(a)–14(c)] show remarkable proximity of the $CO \cdot O_2$ complex to the MgO substrate. Consequently, the interpretation of the enhanced $CO \cdot O_2$ binding at those sites in terms of an attractive $CO \cdot O_2$-MgO interaction arises naturally. Also the high stability of the complex at the type-IV boundary could, in principle, be related to the close proximity to the substrate. In order to substantiate such an assertion, we again proceed to the comparison between adsorption potential energies at both supported and unsupported systems. In Fig. 22 we show the RPBE $CO \cdot O_2$ adsorption potential energies for all four I-IV interfaces, employing either MgO-supported or unsupported cluster boundaries. The $CO \cdot O_2$ binding is clearly enlarged for the supported systems. More interestingly, an apparent correlation between the $CO \cdot O_2$-MgO distance and the magnitude of this effect is found. For the first two cases (a, b), in which the terminal O atom at the $CO \cdot O_2$ group is in close contact with a Mg atom in the topmost MgO layer, the extra binding amounts to around 0.15–0.20 eV. For the type-II situation with oblique orientation, the terminal oxygen is positioned a little further from the substrate, which is reflected in a slightly smaller value of the extra binding $\sim$0.1 eV caused by the substrate. Finally, for the type-III interface the distances involved become very large and the additional $CO \cdot O_2$-MgO binding appears to be only residual $\sim$0.05 eV. The type-IV interface constitutes a very peculiar case; contrary to intuitive expectations, the additional substrate-induced binding is also residual (0.05 eV). Apparently, the

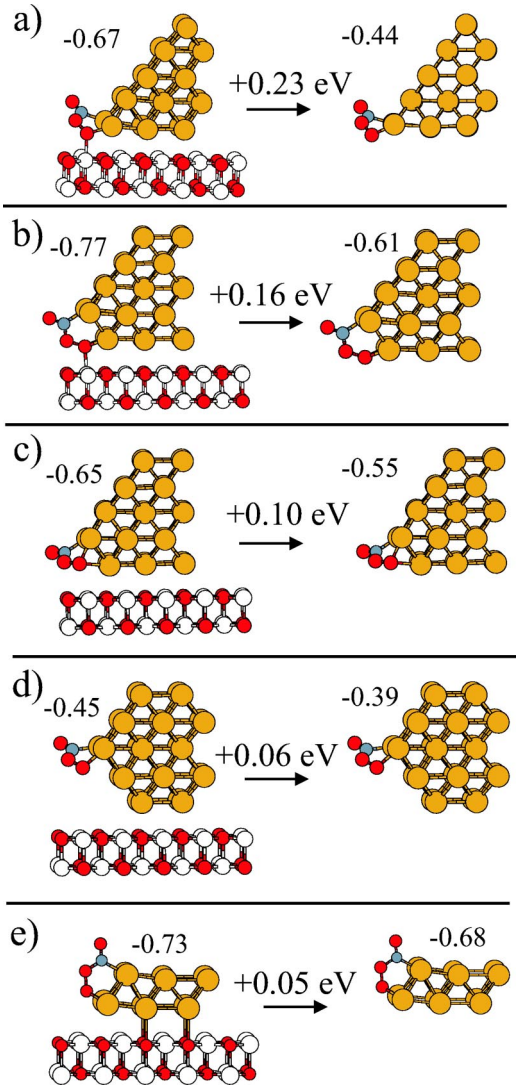

FIG. 22. (Color online) Comparison of RPBE $CO \cdot O_2$ adsorption potential energies (in eV) at supported and unsupported frozen Au cluster boundaries. (a) Type I; (b) type II, perpendicular; (c) type II, oblique; (d) type III; (e) type IV.

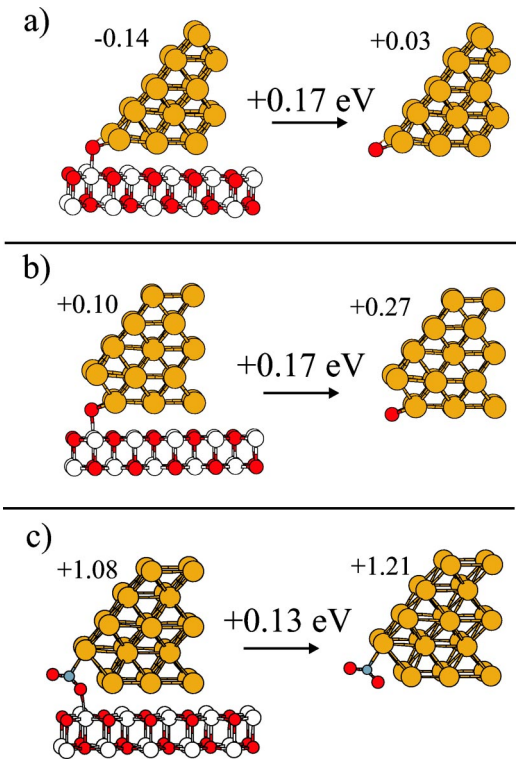

FIG. 23. (Color online) Comparison of RPBE oxygen adsorption potential energies (in eV, positive values indicating endothermic adsorption) at supported and unsupported type-I (a) and type-II (b) cluster boundaries. (c) The same comparison for the metastable state formed during the reaction between CO and adsorbed O at the type-II boundary.

two gold atoms in the lower edge where the terminal oxygen is found are very efficient in "shielding" it from the substrate.

Atomic oxygen adsorbed at the Au-MgO interface behaves very similarly to the terminal oxygen in the $CO \cdot O_2$ intermediate complex. In Fig. 23 the results of a similar set of calculations for O at the type-I and type-II systems are presented, with analogous conclusions. In each case, the oxygen-interface boundary binding strength decreases by 0.17 eV when the substrate is removed. Molecular oxygen, on the other hand, does not behave in this way. A too close contact between adsorbed O_2 and the MgO substrate leads instead to a decrease in the binding. The RPBE adsorption potential energy of O_2 at the type-I interface (+0.21 eV, endothermic) improves slightly to +0.14 eV when the substrate is removed. This also explains the somewhat anomalous adsorption potential energy of +0.2 eV at that site, in contrast to a fairly constant +0.1 eV (endothermic) adsorption potential energy found for the rest of the systems [type-II and-III interfaces, Au(100) and Au(111) facets]. For the type-IV interface, the slightly different geometry of the Au edge in contact with the substrate results in a not so close distance of O_2 to the substrate [see Fig. 8(d)], and consequently no signs of an extra decrease of binding caused by the substrate are seen. Finally, let us comment that the attractive interaction between the terminal oxygen and the oxide is also present for the nearly metastable state formed by CO

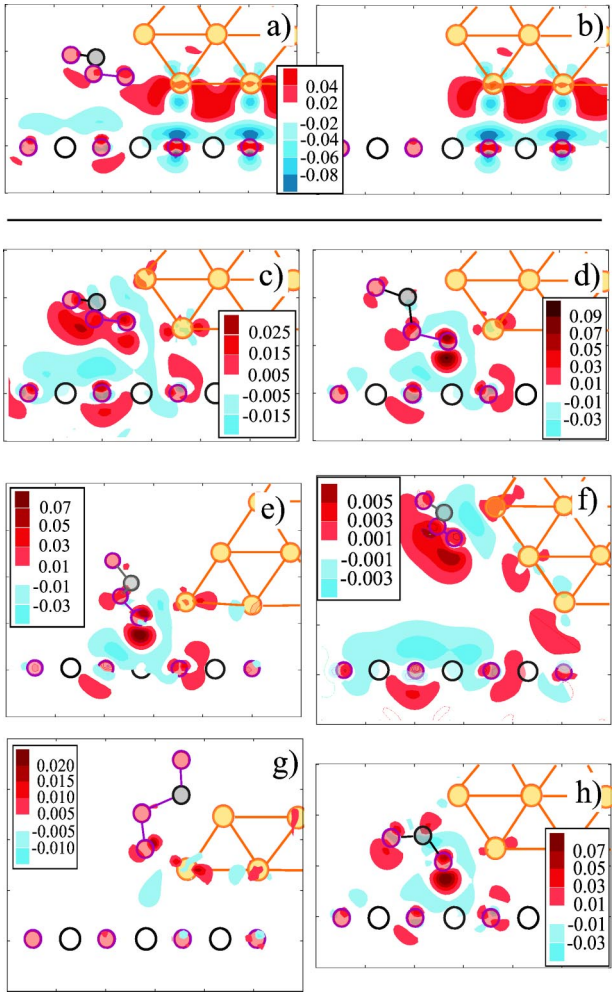

FIG. 24. (Color online) (a,b) Induced charge densities (y-integrated) for the configuration in Fig. 14(c) in units of $e^-/Å^2$; (a) $\varrho_{ads/Au} = \varrho(CO \cdot O_2/Au/MgO) - \varrho(CO \cdot O_2/Au) - \varrho(MgO)$, (b) $\varrho_{Au} = \varrho(Au/MgO) - \varrho(Au) - \varrho(MgO)$. Same scale for both plots. (c–h) Difference in MgO-induced charge densities with and without adsorbate, $\varrho_{ads/Au} - \varrho_{Au}$ for (c) $CO \cdot O_2$ at the type-II interface in its oblique conformer [Fig. 14(c)], (d) the same for the perpendicular orientation [Fig. 14(b)], (e–g) $CO \cdot O_2$ at the type-I, -III, and -IV interfaces, respectively, and (h) nearly metastable $CO \cdot O$ complex at the type-II interface.

and atomic oxygen at the type-II interface (see Sec. IV E). By removing the substrate, the adsorption potential energy of that complex (with respect to CO_2 in the gas phase) changes from +1.08 eV to +1.21 eV, with a net stability loss of 0.13 eV [see Fig. 23(c)]. It must be noted that, even with the extra stabilization induced by the presence of the substrate, the CO-O complex is intrinsically unbound with respect to CO_2(g), and is therefore expected to desorb easily, as is indeed observed.

The effects described above can be very simply understood in terms of electrostatic interactions and charge transfer from the MgO substrate to either the atomic oxygen or the terminal oxygen in $CO \cdot O_2$. In Figs. 24(a) and 24(b) we plot the substrate-induced electron-density profiles for the type-II interface boundary with and without the $CO \cdot O_2$ com-

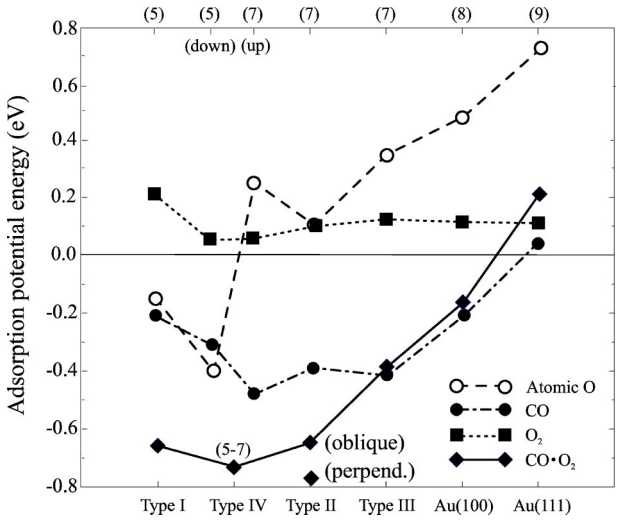

FIG. 25. Adsorption potential energy of CO, O_2, O, and $CO \cdot O_2$ as a function of the Au coordination.

plex adsorbed in the oblique orientation. For the sake of clarity, the 3D electronic densities are averaged along the *y* direction, in the same way as in Fig. 2. In both cases, electrons are seen to flow from the magnesia O^{2-} atoms buried under the Au rod to the first-layer Au atoms. The difference between the two plots reflects the $CO \cdot O_2$-MgO interaction, shown in Fig. 24(c) along with similar plots for the type-I [Fig. 24(e)], type-II (perpendicular conformer, Fig. 24(d), type-III [Fig. 24(f)], and type-IV [Fig. 24(g)] systems. For the type-I and type-II interfaces (both oblique and perpendicular conformers), the presence of the substrate causes the terminal peroxo oxygen atom to accumulate electrons. The magnitude of the effect varies, however. The largest contours appear for the perpendicular conformer at the type-II interface, but the other type-II conformer and the type-I interface also show a strong $CO \cdot O_2$-MgO interaction. The type-III interface shows rather weak complex-support interaction (in terms of the amount of charge transfer) which is easily explained by the large complex-MgO separation occurring for this system. The fact that the complex-MgO distance is indeed a good indicator for the interaction strength is supported by the identification of the shortest distance from the terminal oxygen atom to the support magnesium atom for the system of strongest interaction, i.e., the perpendicular conformer at the type-II interface. Here the OCOO-Mg distance is 2.20 Å, to be compared with the 2.15 Å separating oxygen and magnesium ions in bulk MgO. Finally, in agreement with the energetics reported in Fig. 22(e), the $CO \cdot O_2$ complex at the type-IV interface shows a negligible interaction with the substrate [see Fig. 24(g)].

The same type of charge-transfer effect is also responsible for the enhanced binding of the $CO \cdot O$ nearly-metastable state at the type-II interface shown in Fig. 23(c). In Fig. 24(h) the same *y*-integrated induced charge density is plotted for that situation. The results are completely analogous to the induced charge densities observed for the $CO \cdot O_2$ reaction intermediate in its perpendicular orientation at the same interface [see Fig. 24(d)].

C. The role of coordination

In this section, the relationship between the binding strength of different adsorbates and the Au-Au coordination of the Au sites to which they are attached will be discussed. A correlation between them has been identified in previous theoretical investigations of similar adsorbate-gold systems[11,12] and more general adsorbate-transition and noble-metal systems.[79] This is particularly important for many chemical reactions predicted to occur preferentially at step or kink sites[80–83] In Fig. 25 we plot for several adsorbates the adsorption potential energies versus the Au-Au coordination number of the Au atoms at the adsorption sites. These are fivefold for the type-I interface, both fivefold and sevenfold for the type-IV case, sevenfold for type II and III, and eightfold and ninefold for Au(100) and Au(111), respectively. The adsorption potential energy of O_2 is seen to be essentially independent of the Au coordination. This can be attributed to the absence of a chemical bond in the O_2-Au interaction. For adsorption of CO, O, and $CO \cdot O_2$, where covalent bonds indeed form, a clear trend of increased binding with decreasing coordination is evidenced by the figure.

In the case of CO adsorption, the trend of stronger bonds with smaller coordination is broken for the type-I and type-IV interfaces due to the steric repulsion with the substrate already identified. For O_2, a small repulsion from the MgO builds up over the type-I interface ($+0.2$ eV instead of $+0.1$ eV). This repulsive interaction is responsible for the large activation barrier for the formation of the $CO \cdot O_2$ intermediate in its perpendicular orientation at the type-II interface (~ 0.5 eV, in contrast to the 0.14 eV value for the oblique orientation). In order to attain such perpendicular orientation, O_2 must approach and bind to CO following a pathway too close to the substrate, as discussed in connection with Fig. 16 above.

Combining all the arguments given above, it becomes clear that the special reactivity of the type-II interface can be explained as a combination of favorable circumstances; at this interface, two parallel Au edges meet to provide a variety of stable bonding configurations for the $CO \cdot O_2$ intermediate. Besides, the proximity of the substrate allows for the attractive electrostatic $CO \cdot O_2$-MgO interactions to appear, enhancing even more the ability of CO to bind O_2. Last, but not least, the lifting from the substrate by one Au layer of the low-coordinated Au atoms in the type-II interface with respect to the type-I system helps us to avoid undesirable CO-substrate steric repulsions. The elaborate structure of this highly reactive site resembles the reaction centers in enzymes encountered in biochemistry.[84] Also, such a complicated shape offers a possible reason for the high selectivity found in oxide-supported Au clusters for more complicated reactions including propylene epoxidation and hydrogenation of unsaturated hydrocarbons.[13]

In order to further illustrate the importance of low coordination for the creation of active sites, we have performed an additional calculation of the stability of the $CO \cdot O_2$ intermediate at the type-III interface, now placing it right at the Au-MgO interface in a perpendicular orientation (see Fig. 26), in the same fashion as for the most stable configuration

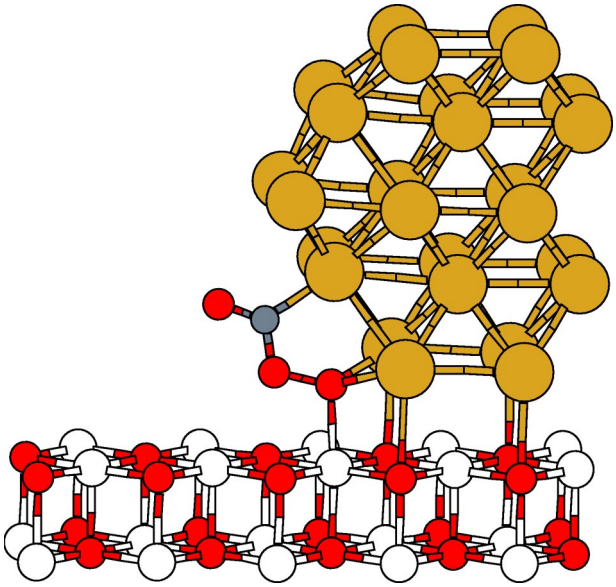

FIG. 26. (Color online) Bonding configuration of $CO \cdot O_2$ at the type-III interface, with the intermediate bound to the substrate.

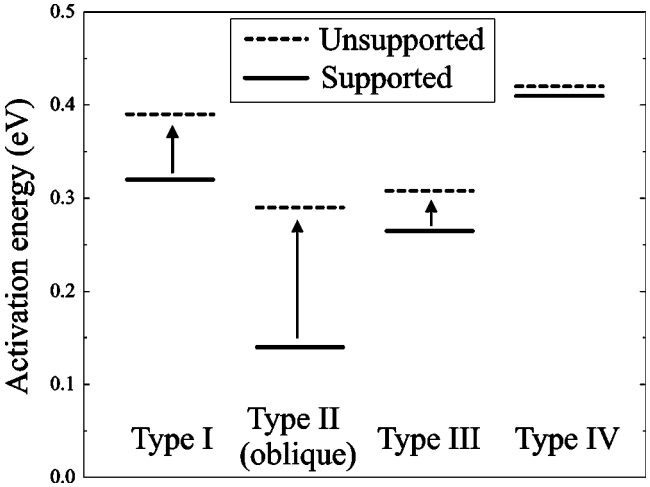

FIG. 27. RPBE activation energies for the formation of $CO \cdot O_2$ at various Au/MgO interfaces, calculated with or without the MgO substrate.

at the type-II interface. The calculation shows that some extra $CO \cdot O_2$-MgO interaction results from moving the complex closer to the substrate; now 0.21 eV is lost upon removing the substrate, while for the most stable configuration [see Fig. 22(d)] only 0.06 eV is lost. Despite this enhanced complex-substrate interaction, the overall adsorption potential energy of the $CO \cdot O_2$ to the Au/MgO system is only -0.27 eV (relative to separate CO and O_2 molecules in the gas phase), which is 0.5 eV less favorable than for the analogous arrangement at the type-II interface (and 0.18 eV less favorable than the most stable arrangement for the type-III interface). Comparing both situations, the main difference between them is the coordination of the Au atom to which CO is attached. This coordination increases from seven (edge atom) for the type-II system to nine (facet atom) for the type-III case of Fig. 26. We see then how the failure of one of the optimum conditions attained for the most favorable system strongly affects the overall reactivity.

Low coordination is an important influence in the case of the type-IV interface. Here, as we have seen, attractive interactions with the MgO substrate play absolutely no role for explaining the high stability of the $CO \cdot O_2$ intermediate at that interface. On the contrary, such high stability is explained by the ability of the intermediate to bind to the edge under very favorable circumstances, with the carbon atom bound to a sevenfold coordinated edge Au atom and the terminal oxygen atom bound at a bridge site between two fivefold coordinated edge Au atoms. Extremely low coordination, a very symmetrical structure, and the favorable fact of the terminal oxygen positioned at a bridge site (test calculations for the binding of a H-O-O- radical to a type-I interface showed a marked preference of around 0.2 eV for the bridging site in contrast to a toplike configuration) result altogether in a rather high overall stability. A comparison of this situation with the one found for the type-I interface is interesting. In the latter case, both carbon and oxygen bind to fivefold coordinated Au atoms; however, now steric repulsion with the substrate [see Figs. 21(e,f)] forbids the $CO \cdot O_2$ complex to rotate around the edge and attain its most favorable orientation. Besides, the terminal oxygen is constrained to bind atop of a Au atom. Although the attractive $CO \cdot O_2$-MgO interaction provides some stabilization for the complex, at the end the overall potential energy (-0.66 eV) is only slightly smaller than the one corresponding to the type-IV case (-0.73 eV). The fact that the reactivity of a given site is a combination of different factors is thereby highlighted; in the case of the type-IV interface, the absence of attractive complex-$CO \cdot O_2$-MgO interaction is compensated by a low Au coordination and a favorable geometry.

D. Effect on the activation energies of the adsorbate-MgO interaction

In order to clarify the origin of the exceptionally low-energy barrier (0.14 eV) obtained for the $CO + O_2$ reaction at the type-II interface (oblique orientation), we have performed an extensive analysis of the influence caused by the presence of the MgO substrate on the potential energies of the transition states found for the reaction at the different Au/MgO interfaces. Following the same procedure of evaluating the potential energies at an *unsupported* Au cluster termination, the analysis can be done accurately by relaxing the structures obtained for the transition states (TS's) for the supported systems (but now without the MgO support) while keeping the C-O bond length frozen at the value for which the TS was found in the supported system. The results for type I-IV interfaces are summarized in Fig. 27. By removing the substrate, we observe that the activation energies for type I-III interfaces increase by various amounts, indicating some attractive interaction between the O_2 molecule (which in every case attains a superoxo state with 1.30–1.35 Å bond lengths and a magnetic moment of the order of 1 μ_B) and the substrate. More interestingly, the type-IV interface does not benefit at all from the presence of the substrate, with

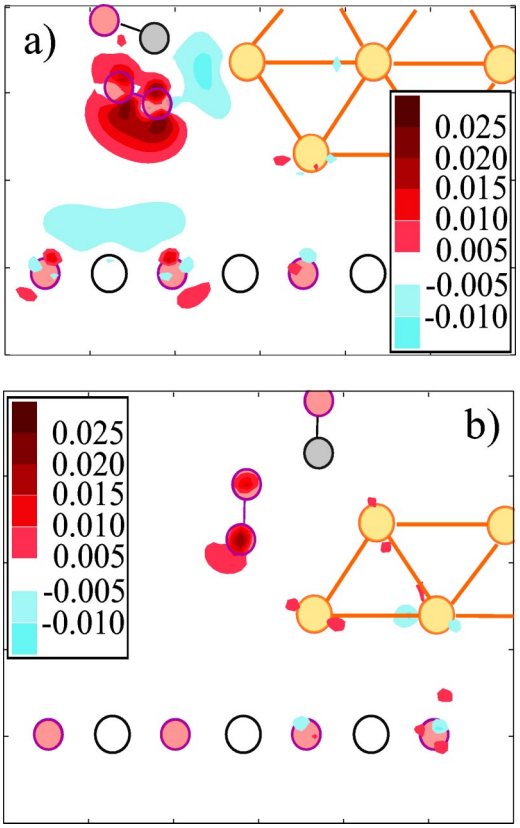

FIG. 28. (Color online) Same as in Fig. 24, for the transition states at the (a) type-II (oblique) and (b) type-IV interfaces.

negligible differences in the energy barrier calculated with or without the substrate. Comparing all four interfaces, the exceptionally low barrier of 0.14 eV at the type-II interface can be largely attributed to a favorable influence of the support.

By performing an induced charge-density study analogous to the ones reported in Sec. V B (oxygen-MgO attractive binding), we find the origin of the enhanced stability of the TS for the type-II interface to be of electrostatic character, involving again a sizable charge transfer from the magnesia O^{2-} anions to the O_2 molecule (see Fig. 28). Therefore, in the case of type-II interfaces, it can be concluded that these attractive interactions are not only responsible for the stabilization of already formed $CO \cdot O_2$ intermediates, but also are extremely important in facilitating its formation. We have also compared the induced charge-density plot obtained for the type-II interface with the one for the type-IV interface, which shows (again) a complete absence of stabilizing oxygen-MgO interactions, a fact which helps us to understand the relatively high (0.4 eV) value of the energy barrier obtained for the type-IV interface.

VI. SUMMARY AND CONCLUSIONS

In the present paper, several important features have been found concerning the structure of Au nanoparticles deposited on MgO, and their ability to catalyze the oxidation of carbon monoxide at low temperature. First, we have calculated relatively low Au-MgO adhesion energies, a finding that strongly suggests a preference for three-dimensional growth of Au on MgO. Furthermore, extremely thin (one atom thick) Au clusters are seen to be energetically very unfavorable, with very small Au clusters found to grow at least two layers thick. For nm-sized particles, epitaxial growth involving the formation of a Au(100)/MgO(100) interface is expected, in agreement with several experiments. The marked preference for Au atoms to be positioned on top of substrate (anionic) oxygen atoms, the corrugation of the potential-energy surface, and the small difference (2%) in lattice parameters between Au and MgO are responsible for this. According to the Wulff-Kaichew construction, this means that the equilibrium shape of Au nanoparticles will be truncated polyhedra. For very small (1–2 nm in diameter) particles, however, calculations show that the actual equilibrium shape may differ from the truncated polyhedral, and truncated square or rectangular pyramids can compete or even be favored. All shapes discussed are the *equilibrium* ones, and the actual shapes appearing for real catalysts can differ substantially from these and show a sizable amount of structural defects, with the possible appearance of multiple-twinned particles. We expect, however, that even in such cases the main conclusions obtained in the present study on the reactivity at different sites around more regular particles would apply.

The interaction of O_2 with Au nanoparticles proved to be very weak, in agreement with the nobleness of gold. Molecular oxygen does not adsorb to Au, and dissociative adsorption is hindered both by unfavorable energetics (in most cases) and by rather high activation barriers. As the interest in Au-supported nanoparticles stems from their ability to catalyze the oxidation of CO at low temperatures (room temperature and below), we focused on the search for alternative pathways not involving O_2 dissociation. Surprisingly, our results show that adsorbed CO is very likely to react with molecular O_2 and form a metastable $CO \cdot O_2$ complex from which CO_2 very easily can be formed. Such a reaction can, in principle, occur at any site around Au nanoparticles (the energy barriers at either edges or facets are never larger than 0.5 eV), but a careful analysis of the reaction energetics indicates that important differences among the different sites indeed exist. Two essential conditions exist that need to be met in order to make such pathways feasible. First, the adsorption of CO must be relatively strong. The calculations have shown that this only happens at low-coordinated edge sites where CO can reversibly adsorb, whereas at either Au(100) or Au(111) facets only a negligible presence of CO can be expected, making these facets essentially inert. An important exception is the case of Au edges in direct contact with the substrate (type-I interfaces) for which steric effects are responsible for an anomalous low binding of CO. From a general perspective, the coordination argument alone helps us to understand why Au particles must be small to be reactive; as it has been already pointed out by Mavrikakis and collaborators,[11] only for very small sizes the amount of edge and corner sites begins to represent a sizable amount of the total number of surface sites in the particle. The second condition is the existence of a sizable driving force for the capture of molecular O_2 and the formation of $CO \cdot O_2$ intermediates. This only occurs at very special places, namely, edges

of the particle placed near the oxide substrate. These places are therefore expected to be highly reactive. The origin of this behavior is the presence of an additional attractive interaction between $CO \cdot O_2$ intermediates and the MgO substrate, which helps not only to stabilize such complexes but also to favor their formation by stabilizing the transition state as well. If we take into account the problems that exist with CO bonding in the case of type-I interfaces, the type-II interfaces are left to be the only sites where both conditions are properly met. We must mention that the type-II interfaces possess also very special geometrical features, bringing together two Au edges and rendering the formation of two different conformers of the $CO \cdot O_2$ intermediate possible. The type-IV interfaces also possess such features on which rather stable $CO \cdot O_2$ intermediates can form; they are hence expected to show sizable reactivity. Besides, the problem with weak CO binding characteristics of the type-I case disappears as strong CO binding is possible at the higher type-IV Au edge. It must however be stressed that, unlike the type-II case, the substrate cannot stabilize the transition state for the formation of $CO \cdot O_2$, which results in a higher activation energy and therefore an expected smaller reactivity at the type-IV interface. Finally, given the high activity found towards CO adsorption, any corner site (and specially the ones near MgO) can presumably be active as well for the $CO(ads) + O_2(g)$ reaction.

Adding these results to the expected evolution of the shape of a supported cluster as a function of size (derived from the Wulff-Kaichew construction and the results obtained in Sec. III), it can be concluded that a certain critical size exists at which the Au particles are expected to be highly reactive. According to experiments, this happens for diameters around 2–3 nm, where a high concentration of low-coordinated surface sites occurs and the interface boundary is likely to resemble our type-II model. The theoretical results also agree with the larger activities observed for hemispherical Au particles, in contrast to spherical ones.[13]

Finally, another interesting result is the highly reactive character of atomic oxygen adsorbed on Au particles. The fact that this adsorbate is not very tightly bound to Au allows for an easy removal by CO with negligible or no barriers at all. We believe that this behavior is closely related to the ability of Au to catalyze oxidation reactions *at low temperature*. More ''active'' transition metals (such as Pt) can very easily dissociate O_2 and bind strongly both atomic oxygen and CO, which in principle must facilitate the reaction. At the same time, however, such more tightly bound adsorbates are expected to overcome sizable barriers to react, rendering the reaction rates to be significant only at higher temperatures. On the contrary, gold appears as a special case where the reactants are rather loosely bound (and only under very special circumstances; in most cases, e.g., at the facets, they do not bind at all). This means that if special requirements are met, the adsorbates are likely to react with very small activation energies, making the reaction possible at very low temperatures.

ACKNOWLEDGMENTS

This work was supported by The Danish Research Councils and Dansk Center for Scientific Computing. We thank Jeanette Dandanell for proofreading the manuscript.

[1] M. Haruta, T. Kobayashi, H. Sano, and N. Yamada, Chem. Lett. **2**, 405 (1987).
[2] M. Haruta, Catal. Today **36**, 153 (1997).
[3] T.M. Hayashi, K. Tanaka, and M. Haruta, J. Catal. **178**, 566 (1998).
[4] T. Salama, R. Ohnishi, T. Shido, and M. Ichikawa, J. Catal. **162**, 169 (1996).
[5] J.A. Rodriguez, G. Liu, T. Jirsak, J. Hrbek, Z.P. Chang, J. Dvorak, and A. Maiti, J. Am. Chem. Soc. **124**, 5242 (2002).
[6] A. Wolf and F. Schüth, Appl. Catal. A Gen. **226**, 1 (2002).
[7] M.M. Schubert, S. Hackenberg, A.C. van Veen, M. Muhler, V. Plzak, and R.J. Behm, J. Catal. **197**, 113 (2001).
[8] N. Lopez, T.V.W. Janssens, B.S. Clausen, Y. Xu, M. Mavrikakis, T. Bligaard, and J.K. Nørskov, J. Catal. **223**, 232 (2004).
[9] M. Valden, X. Lai, and D.W. Goodman, Science **281**, 1647 (1998).
[10] V.A. Bondzie, S.C. Parker, and C.T. Campbell, J. Vac. Sci. Technol. A **17**, 1717 (1999).
[11] M. Mavrikakis, P. Stoltze, and J.K. Nørskov, Catal. Lett. **64**, 101 (2000).
[12] N. Lopez and J.K. Nørskov, J. Am. Chem. Soc. **124**, 11262 (2002).
[13] M. Haruta, CATTECH **6**, 102 (2002).
[14] J.J. Pietron, R.M. Stroud, and D.R. Rolison, Nano Lett. **2**, 545 (2002).
[15] G.C. Bond and D.T. Thompson, Gold Bull. (Geneva) **33**, 41 (2001).
[16] C. Stampfl and M. Scheffler, Phys. Rev. Lett. **78**, 1500 (1997).
[17] A. Alavi, P. Hu, T. Deutsch, P.L. Silvestrelli, and J. Hutter, Phys. Rev. Lett. **80**, 3650 (1998).
[18] A. Eichler and J. Hafner, Surf. Sci. **435**, 58 (1999).
[19] C.C. Cudia, S.W. Hla, G. Comelli, Ž. Šljivančanin, B. Hammer, A. Baraldi, K.C. Prince, and R. Rosei, Phys. Rev. Lett. **87**, 196104 (2001).
[20] C.J. Zhang and P. Hu, J. Am. Chem. Soc. **122**, 2134 (2000).
[21] C.J. Zhang, P. Hu, and A. Alavi, J. Chem. Phys. **114**, 8113 (2001).
[22] B. Hammer, J. Catal. **199**, 171 (2001).
[23] Z.-P. Liu, X.-Q. Gong, J. Kohanoff, C. Sanchez, and P. Hu, Phys. Rev. Lett. **91**, 266102 (2003).
[24] R.J.H. Grisel and B.E. Nieuwenhuys, J. Catal. **199**, 48 (2001).
[25] A. Sanchez, S. Abbet, U. Heiz, W.D. Schneider, H. Häkkinen, R.N. Barnett, and U. Landman, J. Phys. Chem. A **103**, 9573 (1999).
[26] G. Mills, M.S. Gordon, and H. Metiu, Chem. Phys. Lett. **359**, 493 (2002).
[27] B. Yoon, H. Häkkinen, and U. Landman, J. Phys. Chem. A **107**, 4066 (2003).
[28] B.E. Salisbury, W.T. Wallace, and R.L. Whetten, Chem. Phys. **262**, 131 (2000).

[29] L.M. Molina and B. Hammer, Phys. Rev. Lett. **90**, 206102 (2003).
[30] M.C. Payne, M.P. Teter, D.C. Allan, T.A. Arias, and J.D. Joannopoulos, Rev. Mod. Phys. **64**, 1045 (1992).
[31] D. Vanderbilt, Phys. Rev. B **41**, 7892 (1990).
[32] B. Hammer, L.B. Hansen, and J.K. Nørskov, Phys. Rev. B **59**, 7413 (1999).
[33] S. Kurth, J.P. Perdew, and P. Blaha, Int. J. Quantum Chem. **75**, 889 (1999).
[34] J.P. Perdew, J.A. Chevary, S.H. Vosko, K.A. Jackson, M.R. Pederson, D.J. Singh, and C. Fiolhais, Phys. Rev. B **46**, 6671 (1992).
[35] Y. Zhang and W. Yang, Phys. Rev. Lett. **80**, 890 (1998).
[36] D.C. Liu and J. Nocedal, Math. Program. **45**, 503 (1989).
[37] F. Furche, R. Ahlrichs, P. Weis, C. Jacob, S. Gilb, T. Bierweiler, and M.M. Kappes, J. Chem. Phys. **117**, 6982 (2002).
[38] H. Häkkinen and U. Landman, Phys. Rev. B **62**, R2287 (2000).
[39] M. José Yacamán, J.A. Ascencio, H.B. Liu, and J. Gardea-Torresdey, J. Vac. Sci. Technol. B **19**, 1091 (2001).
[40] J. Li, X. Li, H.J. Zhai, and L.S. Wang, Science **299**, 864 (2003).
[41] T. Kizuka and N. Tanaka, Phys. Rev. B **56**, 10 079 (1997).
[42] B. Pauwels, G. Van Tendeloo, W. Bouwen, L.T. Kuhn, P. Lievens, H. Lei, and M. Hou, Phys. Rev. B **62**, 10 383 (2000).
[43] P.M. Ajayan and L.D. Marks, Nature (London) **338**, 139 (1989).
[44] S. Giorgio, C. Chapon, C.R. Henry, G. Nihoul, and J.M. Penisson, Philos. Mag. A **64**, 87 (1991).
[45] H. Häkkinen, M. Moseler, and U. Landman, Phys. Rev. Lett. **89**, 033401 (2002).
[46] F. Furche, R. Ahlrichs, P. Weis, C. Jacob, S. Gilb, T. Bierweiler, and M.M. Kappes, J. Chem. Phys. **117**, 6982 (2002).
[47] A. Vittadini and A. Selloni, J. Chem. Phys. **117**, 353 (2002).
[48] I. Yudanov, G. Pacchioni, K. Neyman, and N. Rösch, J. Phys. Chem. B **101**, 2786 (1997).
[49] A. Bogicevic and D.R. Jennison, Phys. Rev. Lett. **82**, 4050 (1999).
[50] A.E. Mattsson and W. Kohn, J. Chem. Phys. **115**, 3441 (2001).
[51] A.E. Mattsson and D.R. Jennison, Surf. Sci. **520**, L611 (2002).
[52] G. Wulff, Z. Kristallogr. **34**, 449 (1901).
[53] W.L. Winterbottom, Acta Metall. **15**, 303 (1967).
[54] P.L. Hansen, J.B. Wagner, S. Helveg, J.R. Rostrup-Nielsen, B.S. Clausen, and H. Topsøe, Science **295**, 2053 (2002).
[55] A.N. Patil, D.Y. Paithankar, N. Otsuka, and R.P. Andres, Z. Phys. D: At., Mol. Clusters **26**, 135 (1993).
[56] C.L. Cleveland, U. Landman, T.G. Schaaff, M.N. Shafigullin, P.W. Stephens, and R.L. Whetten, Phys. Rev. Lett. **79**, 1873 (1997).
[57] D. Lovall, M. Buss, R.P. Andres, and R. Reifenberger, Phys. Rev. B **58**, 15 889 (1998).
[58] K.H. Hansen, T. Worren, S. Stempel, E. Laegsgaard, M. Baumer, H.J. Freund, F. Besenbacher, and I. Stensgaard, Phys. Rev. Lett. **83**, 4120 (1999).
[59] H. Graoui, S. Giorgio, and C.R. Henry, Philos. Mag. B **81**, 1649 (2001).
[60] W. Vervisch, C. Mottet, and J. Goniakowski, Phys. Rev. B **65**, 245411 (2002).
[61] C.L. Cleveland, U. Landman, and M.N. Shafigullin, Z. Phys. D: At., Mol. Clusters **40**, 503 (1997).
[62] K. Reuter and M. Scheffler, Phys. Rev. Lett. **90**, 046103 (2003).
[63] W.X. Li, C. Stampfl, and M. Scheffler, Phys. Rev. Lett. **90**, 256102 (2003).
[64] E. Lundgren, G. Kresse, C. Klein, M. Borg, J.N. Andersen, M. De Santis, Y. Gauthier, C. Konvicka, M. Schmid, and P. Varga, Phys. Rev. Lett. **88**, 246103 (2002).
[65] B.L.M. Hendriksen and J.W.M. Frenken, Phys. Rev. Lett. **89**, 046101 (2002).
[66] S. Surnev, J. Schoiswohl, G. Kresse, M.G. Ramsey, and F.P. Netzer, Phys. Rev. Lett. **89**, 246101 (2002).
[67] A. Eichler and J. Hafner, Phys. Rev. Lett. **79**, 4481 (1997).
[68] M.-L. Bocquet, J. Cerda, and P. Sautet, Phys. Rev. B **59**, 15 437 (1999).
[69] P.J. Feibelman, Phys. Rev. B **59**, 2327 (1999).
[70] B. Hammer and J. Nørskov, Nature (London) **376**, 238 (1995).
[71] B. Hammer, Phys. Rev. Lett. **89**, 016102 (2002).
[72] X. Wu, L. Senapati, S.K. Nayak, A. Selloni, and M. Hajaligol, J. Chem. Phys. **117**, 4010 (2002).
[73] F. Boccuzzi, A. Chiorino, M. Manzoli, P. Lu, T. Akita, S. Ichikawa, and M. Haruta, J. Catal. **202**, 256 (2001).
[74] Sh.K. Shaikhutdinov, R. Meyer, M. Naschitzki, M. Bäumer, and H.-J. Freund, Catal. Lett. **86**, 211 (2003).
[75] H. Huber, D. McIntosh, and G.A. Ozin, Inorg. Chem. **16**, 975 (1977).
[76] W.T. Wallace and R.L. Whetten, J. Am. Chem. Soc. **124**, 7499 (2002).
[77] J. Hagen, L.D. Socaciu, M. Elijazyfer, U. Heiz, T.M. Bernhardt, and L. Wöste, Phys. Chem. Chem. Phys. **4**, 1707 (2002).
[78] Z.-P. Liu, P. Hu, and A. Alavi, J. Am. Chem. Soc. **124**, 14770 (2002).
[79] B. Hammer and J. Nørskov, Adv. Catal. **45**, 71 (2000).
[80] T. Zambelli, J. Wintterlin, J. Trost, and G. Ertl, Science **273**, 1688 (1996).
[81] S. Dahl, A. Logadottir, R.C. Egeberg, J.H. Larsen, I. Chorkendorff, E. Törnqvist, and J.K. Nørskov, Phys. Rev. Lett. **83**, 1814 (1999).
[82] B. Hammer, Phys. Rev. Lett. **83**, 3681 (1999).
[83] P. Gambardella, Ž. Šljivančanin, B. Hammer, M. Blanc, K. Kuhnke, and K. Kern, Phys. Rev. Lett. **87**, 056103 (2001).
[84] L. Stryer, *Biochemistry* (Freeman, New York, 1999).